Mathematics

https://www.aimspress.com/journal/Math

AIMS Mathematics, 11(9): 28318–28347.
DOI: 10.3934/math.20261128
Received: 22 July 2026
Revised: 21 August 2026
Accepted: 26 August 2026
Published: 04 September 2026

Research article

Mathematical modeling and analysis of controlled fractional RC and RLC circuits with generalized memory kernels and uncertainty quantification

Ishtiaq Ali*

Department of Mathematics and Statistics, College of Science, King Faisal University, P.O. Box 400, Al-Ahsa, 31982, Saudi Arabia

* **Correspondence:** Email: iamirzada@kfu.edu.sa.

Abstract: This paper presents a common kernel-dependent mathematical framework for modeling and analyzing controlled fractional resistor–capacitor (RC) and resistor–inductor–capacitor (RLC) circuits using several singular and nonsingular memory kernels. The proposed models describe hereditary and nonlocal memory effects in transient, oscillatory, and damping behaviors under constant and periodic excitations, with a characteristic dimensional scaling parameter introduced to preserve physical consistency in the fractional-order formulation. Analytical solutions are derived using Laplace transform techniques and generalized Mittag–Leffler functions, providing explicit representations of the circuit responses for different fractional operators. A fractional-order proportional–integral (PI) controller is incorporated to suppress oscillations, reduce overshoot, enhance damping, and accelerate convergence toward the corresponding equilibrium or bounded periodic regime. To assess the robustness of the proposed models, uncertainty quantification based on Monte Carlo (MC) simulations is employed under stochastic variations in fractional orders, relaxation parameters, damping coefficients, oscillation frequencies, and controller gains. Numerical results demonstrate the significant influence of the memory kernels and fractional orders on the dynamical behavior of the circuits, and the proposed control strategy consistently improves transient responses. Furthermore, the uncertainty analysis shows that the stochastic responses remain bounded and closely follow the corresponding deterministic controlled trajectories, indicating robust behavior of the proposed mathematical framework under the considered parameter perturbations.

Keywords: mathematical modeling; generalized memory kernels; fractional RC and RLC circuits; fractional–order control; dynamical analysis; uncertainty quantification
Mathematics Subject Classification: 26A33, 34A08, 34C60

1. Introduction

Fractional calculus has become an important mathematical tool for modeling physical systems involving memory effects, hereditary properties, anomalous diffusion, and nonlocal interactions. Unlike classical integer-order models, fractional differential equations provide a more realistic representation of many engineering and scientific processes in which the current state of the system depends on its previous history [1, 2]. Fractional calculus has very important applications in electrical circuits, as practical electrical components present nonideal behaviors such as dielectric polarization, thermal memory, electromagnetic hysteresis, anomalous charge transport, and dissipative energy effects [3, 4]. These physical phenomena cannot be accurately modeled by classical resistor–capacitor (RC) and resistor–inductor–capacitor (RLC) circuit models with only integer-order derivatives. Therefore, fractional–order electrical circuits have received much attention in electrical engineering, signal processing, electrochemical systems, viscoelastic electronics, and energy storage devices [5–7]. Fractional derivatives are used in electrical circuit modeling to capture memory and hereditary properties of various system components via nonlocal operators. Among the most popular operators is the Liouville–Caputo fractional derivative because of its great ability to describe power law memory behavior and relaxation phenomena [8]. Many works have been devoted to studying the fractional RC, resistor-inductor (RL), and RLC circuits under different forcing conditions and excitation sources based on this operator [9–11]. Valsa and Vlach [12] analyzed the transient response of fractional electrical systems and their practical realizations. Fractional electrical models have also been successfully applied to supercapacitors, dielectric materials, bioimpedance systems, and signal filtering problems [13, 14].

Although the classical Caputo derivative has been extensively used in electrical engineering, several generalized fractional operators with singular and nonsingular kernels have recently been proposed to improve the modeling of memory-dependent physical systems. Caputo and Fabrizio introduced a fractional derivative with an exponential nonsingular kernel in order to avoid the singularity associated with the classical power law kernel [15]. Further mathematical properties and applications of this operator were investigated in [16]. Then, Atangana and Baleanu introduced a generalized fractional derivative with the Mittag–Leffler kernel, which provides a more flexible description of crossover memory effects and anomalous relaxation dynamics [17]. Later, Atangana and Koca [18] introduced another fractional operator generalized with the generalized Mittag-Leffler function. On the other hand, Khalil et al. introduced the conformable derivative, which keeps some classical properties of ordinary differentiation such as the product rule, quotient rule, and chain rule [19]. Jarad et al. have further developed this idea by introducing fractional conformable operators that depend on two fractional parameters (α, β) and that offer higher flexibility to describe multiscale memory effects in physical systems [20]. Many fractional electrical models have analytical solutions closely related to the Mittag-Leffler function, which is of fundamental importance for the description of fractional relaxation and oscillatory processes [21].

In recent years, important advances have also been made in the analysis and simulation of fractional electrical circuits. The transient responses, resonance behavior, damping characteristics, and stability properties of fractional RC and RLC systems have been studied in the literature using several analytical, numerical, and computational methods [22, 23]. However, most of the existing works do not consider advanced control mechanisms or uncertainty analysis and focus on obtaining analytical solutions or comparing different fractional kernels. In practice, in electrical systems, there are uncertainties due to parameter perturbations, manufacturing tolerances, thermal fluctuations, external disturbances, and measurement errors. However, uncertainty quantification for generalized fractional electrical circuits remains underexplored in the literature. Moreover, fractional-order control has been proved to work efficiently in engineering systems and dynamical models [24] but fractional-order control, along with generalized fractional RC and RLC circuit models with singular and nonsingular operators, has not been studied sufficiently.

Fractional electrical circuits have received much attention due to their ability to model memory and hereditary effects more accurately than classical integer-order models. Gómez-Aguilar et al. [25] investigated fractional RC and inductor–capacitor (LC) electrical circuits and demonstrated the relevance of fractional-order formulations for describing electrical responses with memory effects. Morales-Delgado et al. [26] derived analytical solutions for electrical circuits described by fractional conformable derivatives in the Liouville–Caputo sense. More recently, experimental studies by Lin et al. [27] using the Caputo and Caputo–Fabrizio derivatives showed that fractional RC circuit models provide improved characterization of nonlocal electrical dynamics and agreement with experimental electrical behavior. Also, efficient numerical algorithms based on Fibonacci wavelets and Legendre pseudospectral methods were developed for fractional RL, RC, and RLC circuits, demonstrating their high accuracy and computational efficiency to solve fractional dynamical systems [28, 29]. Furthermore, nonlinear dynamical analysis revealed that coupled systems with memory and delay effects could display complex bifurcation structures and rich dynamical behaviors [30]. Moreover, electrical circuits described by fractional derivatives with singular and nonsingular kernels have been widely investigated [31]. These developments motivate the present work to further investigate the dynamics of fractional RC and RLC circuits with fractional-order control strategies and uncertainty quantification to analyze robustness, frequency response, and energy dissipation under different memory kernels.

More recently, fractional calculus has been applied more and more to the modeling of electrical circuits. In advanced analytical studies, it has been shown that fractional order RC models offer more flexibility and more accurate behavioral description than classical integer order formulations [32]. Fractional RL and RC circuits have also been solved accurately using semianalytical methods, which have proven to be able to capture nonlocal electrical responses [33]. Recent computational developments include the radial basis function neural network approach of Liu and Ding for solving diffusion partial differential equations, with the potential of learning-assisted methods for differential equation models [34]. Spectral uncertainty quantification methods have also been motivated by random parameter perturbations. Duong and Lee applied polynomial chaos to a fractional-order PI control system [35]. González–Parra et al. developed a generalized polynomial chaos (gPC) framework for random fractional-order differential equations as an efficient alternative to Monte Carlo sampling [36]. Most recently, Jornet used gPC expansions and stochastic Galerkin projection for random fractional Bateman equations, and provided mean and variance approximations validated against Monte Carlo simulations [37]. These studies show the efficiency of polynomial-chaos techniques for the propagation of uncertainty in fractional-order dynamical systems.

These observations motivate a unifying multikernel framework for fractional RC and RLC circuits that combines fractional order control with uncertainty quantification. In this work, we consider the Liouville–Caputo, Caputo–Fabrizio, Atangana–Baleanu–Caputo, Atangana–Koca–Caputo, conformable, and fractional-conformable operators. By means of Laplace transforms and generalized Mittag–Leffler functions, analytical solutions for charging, discharging, and periodically excited circuits are derived. Fractional–order control is presented to increase damping, reduce overshoot, and speed up the convergence to equilibrium or bounded periodic regimes. Monte Carlo simulations are used to quantify parameter uncertainty, including fractional parameters, damping coefficients, oscillation frequencies and controller gains. Numerical results are then used to compare the fractional operators and to evaluate the combined effects of memory, control, and uncertainty on the transient and oscillatory dynamics of the circuit.

The remainder of the paper is organized as follows. Section 2 presents the mathematical preliminaries and definitions of the fractional operators used in this work. Section 3 introduces the generalized fractional RC and RLC circuit models together with the proposed fractional-order control and uncertainty quantification framework. Section 4 presents the analytical solutions of the proposed fractional circuit models. Section 5 is devoted to the results and discussion. Finally, concluding remarks are presented in Section 6.

2. Mathematical preliminaries

In this section, the generalized fractional operators, special functions, fractional–order control strategy, and uncertainty quantification framework required for the proposed electrical circuit models are introduced. The considered operators involve both singular and nonsingular memory kernels and provide a unified mathematical framework for modeling hereditary effects, anomalous relaxation, and nonlocal electrical dynamics. In contrast to classical integer-order formulations, the present framework incorporates memory-dependent dissipation, fractional damping behavior, and stochastic parameter variability within controlled RC and RLC electrical systems.

2.1. Generalized fractional operators

Let $\psi(\tau)$ be sufficiently smooth on the interval $[0, T]$. The generalized fractional electrical models considered in this work are constructed using several fractional operators associated with different memory kernels. Throughout this work, ϑ denotes the fractional order of the generalized Caputo, Caputo–Fabrizio, Atangana–Baleanu, and Atangana–Koca operators. The fractional operators are introduced here in their standard mathematical forms; dimensional consistency of their application to the electrical circuit models is enforced subsequently through a characteristic time-scaling parameter σ_0 in the fractionalized circuit equations.

Definition 2.1. *The generalized Caputo fractional derivative of order ϑ is defined by*

$$ {}^{\mathrm{GC}}\mathcal{D}_{\tau}^{\vartheta}\psi(\tau) = \frac{1}{\Gamma(m-\vartheta)} \int_0^{\tau} (\tau-\xi)^{m-\vartheta-1}\psi^{(m)}(\xi)\, d\xi, \qquad m-1 < \vartheta < m. \tag{2.1}$$

Its Laplace transform is given by

$$\mathcal{L}\left\{ {}^{\mathrm{GC}}\mathcal{D}_{\tau}^{\vartheta}\psi(\tau)\right\} = s^{\vartheta}\Psi(s) - \sum_{j=0}^{m-1} s^{\vartheta-j-1}\psi^{(j)}(0), \tag{2.2}$$

where

$$\Psi(s) = \mathcal{L}\{\psi(\tau)\}.$$

Definition 2.2. *The Caputo–Fabrizio fractional derivative of order ϑ with an exponential nonsingular kernel is defined by*

$$ {}^{\mathrm{CF}}\mathcal{D}_{\tau}^{\vartheta}\psi(\tau) = \frac{\mathcal{N}(\vartheta)}{1-\vartheta}\int_0^{\tau}\psi'(\xi)\exp\left(-\frac{\vartheta}{1-\vartheta}(\tau-\xi)\right)d\xi, \qquad 0<\vartheta<1, \tag{2.3}$$

where $\mathcal{N}(\vartheta)$ is the normalization function satisfying

$$\mathcal{N}(0)=\mathcal{N}(1)=1.$$

Its corresponding Laplace transform is

$$\mathcal{L}\left\{{}^{\mathrm{CF}}\mathcal{D}_{\tau}^{\vartheta}\psi(\tau)\right\} = \frac{\mathcal{N}(\vartheta)}{(1-\vartheta)s+\vartheta}\left[s\Psi(s)-\psi(0)\right]. \tag{2.4}$$

Definition 2.3. *The Atangana–Baleanu fractional derivative of order ϑ in the Caputo sense is defined by*

$$ {}^{\mathrm{AB}}\mathcal{D}_{\tau}^{\vartheta}\psi(\tau) = \frac{\mathcal{B}(\vartheta)}{1-\vartheta}\int_0^{\tau}\psi'(\xi)E_{\vartheta}\left(-\frac{\vartheta}{1-\vartheta}(\tau-\xi)^{\vartheta}\right)d\xi, \qquad 0<\vartheta<1, \tag{2.5}$$

where $\mathcal{B}(\vartheta)$ is the normalization function satisfying

$$\mathcal{B}(0)=\mathcal{B}(1)=1.$$

Its corresponding Laplace transform is

$$\mathcal{L}\left\{{}^{\mathrm{AB}}\mathcal{D}_{\tau}^{\vartheta}\psi(\tau)\right\} = \frac{\mathcal{B}(\vartheta)}{1-\vartheta}\frac{s^{\vartheta}\Psi(s)-s^{\vartheta-1}\psi(0)}{s^{\vartheta}+\dfrac{\vartheta}{1-\vartheta}}. \tag{2.6}$$

Definition 2.4. *Let $\psi\in H^1(0,T)$, and $0<\vartheta\le 1$. The Atangana–Koca fractional derivative of order ϑ in the Caputo sense is defined by*

$$ {}^{\mathrm{AK}}\mathcal{D}_{\tau}^{\vartheta}\psi(\tau) = \frac{1}{\chi(\vartheta)}\int_0^{\tau}\psi'(\xi)E_{\vartheta,\vartheta}^{\vartheta}\left(-\chi(\vartheta)(\tau-\xi)^{\vartheta}\right)d\xi, \qquad 0<\vartheta\le 1, \tag{2.7}$$

where $\chi(\vartheta)$ is a normalization function, and $E_{\alpha,\beta}^{\gamma}(z)$ denotes the three-parameter generalized Mittag–Leffler function defined by

$$E_{\alpha,\beta}^{\gamma}(z) = \sum_{k=0}^{\infty}\frac{(\gamma)_k}{k!\,\Gamma(\alpha k+\beta)}z^k, \tag{2.8}$$

with $(\gamma)_k=\Gamma(\gamma+k)/\Gamma(\gamma)$ denoting the Pochhammer symbol.

Definition 2.5. *The generalized conformable derivative of order $\rho\in(0,1)$ is defined by*

$$\mathcal{T}_{\tau}^{\rho}\psi(\tau) = \lim_{\varepsilon\to 0}\frac{\psi\left(\tau+\varepsilon\tau^{1-\rho}\right)-\psi(\tau)}{\varepsilon}, \qquad \tau>0. \tag{2.9}$$

Definition 2.6. *The fractional conformable derivative of orders ρ and σ in the Liouville–Caputo sense is defined by*

$$ {}^{\mathrm{FC}}\mathcal{D}_{\tau}^{\rho,\sigma}\psi(\tau) = \frac{1}{\Gamma(m-\sigma)}\int_0^{\tau}\left(\frac{\tau^{\rho}-\xi^{\rho}}{\rho}\right)^{m-\sigma-1}\mathcal{T}_{\xi}^{m\rho}\psi(\xi)\frac{d\xi}{\xi^{1-\rho}}, \qquad 0<\rho\le 1, \qquad m-1<\sigma<m. \tag{2.10}$$

The above operators represent different classes of memory kernels, including singular power law kernels, exponential non-singular kernels, generalized Mittag–Leffler kernels, and local conformable kernels. Throughout this work, ϑ denotes the fractional order of the generalized Caputo, Caputo–Fabrizio, Atangana–Baleanu, and Atangana–Koca operators, whereas ρ and σ denote the conformable and fractional orders, respectively, of the fractional conformable operator. These operators provide different relaxation characteristics and damping behaviors for modeling hereditary electrical systems and anomalous energy–dissipation processes.

2.2. Regularity and applicability of the memory kernels

The fractional operators employed in this work are characterized by kernels with distinct regularity and memory-decay properties. For the Liouville–Caputo operator with $0 < \vartheta < 1$, the convolution kernel is

$$K_\vartheta^{\mathrm{C}}(\tau) = \frac{\tau^{-\vartheta}}{\Gamma(1-\vartheta)}.$$

Although K_ϑ^{C} is singular at $\tau = 0$, the singularity is integrable on every finite interval. Indeed,

$$K_\vartheta^{\mathrm{C}} \in L^1(0,T), \qquad \int_0^T \left|K_\vartheta^{\mathrm{C}}(\tau)\right| d\tau = \frac{T^{1-\vartheta}}{\Gamma(2-\vartheta)} < \infty.$$

Therefore, if $\psi \in AC[0,T]$, then $\psi' \in L^1(0,T)$ and the Liouville–Caputo derivative, expressed as the convolution of K_ϑ^{C} with ψ', is well–defined almost everywhere on $(0,T]$. The weak singularity of the kernel is thus compatible with the regularity assumed for the circuit state variables.

For the Caputo–Fabrizio operator, the kernel

$$K_\vartheta^{\mathrm{CF}}(\tau) = \frac{N(\vartheta)}{1-\vartheta}\exp\left(-\frac{\vartheta}{1-\vartheta}\tau\right)$$

is nonsingular, continuous, and bounded on every finite interval for each fixed $0 < \vartheta < 1$, provided that the normalization function $N(\vartheta)$ is finite. The corresponding memory therefore decays exponentially with the elapsed time τ.

Similarly, the Atangana–Baleanu kernel

$$K_\vartheta^{\mathrm{AB}}(\tau) = \frac{B(\vartheta)}{1-\vartheta}E_\vartheta\left(-\frac{\vartheta}{1-\vartheta}\tau^\vartheta\right)$$

is nonsingular and continuous on finite intervals for fixed $0 < \vartheta < 1$, provided that $B(\vartheta)$ is finite and positive. Because $E_\vartheta(0) = 1$, its value at the origin is finite, and no power law singularity occurs there.

For the generalized Atangana–Koca formulation considered here, the kernel

$$K_\vartheta^{\mathrm{AK}}(\tau) = \frac{1}{\chi(\vartheta)}E_{\vartheta,\vartheta}^{\vartheta}\left(-\chi(\vartheta)\tau^\vartheta\right)$$

is also nonsingular at the origin when $\chi(\vartheta)$ is finite and nonzero. In particular,

$$K_\vartheta^{\mathrm{AK}}(0) = \frac{1}{\chi(\vartheta)\Gamma(\vartheta)},$$

which is finite for $0 < \vartheta < 1$. Hence, the Caputo–Fabrizio, Atangana–Baleanu, and Atangana–Koca kernels define regular memory convolutions on finite time intervals under the regularity assumptions adopted for the circuit variables.

The conformable operator has a different mathematical structure from the preceding operators. It is local in time and does not contain an explicit history convolution. Consequently, its fractional behavior arises through the local time-dependent scaling of the derivative rather than through a hereditary memory kernel. The fractional-conformable operator used in this work combines conformable scaling with a fractional integral structure and is well-defined whenever the weighted integral appearing in Definition 2.6 exists and the corresponding conformable derivatives satisfy the required regularity conditions.

Different kernel structures correspond to different types of temporal memory. The Liouville–Caputo kernel describes long–range power law memory, the Caputo–Fabrizio kernel describes exponential memory decay, and the Atangana–Baleanu and Atangana–Koca kernels are nonsingular Mittag–Leffler-type kernels, whereas conformable operators describe local fractional time scaling. These differences affect transient decay, oscillation amplitude, phase behavior, and convergence in RC and RLC circuits. From an engineering perspective, kernel selection should therefore reflect the experimentally observed relaxation and dissipation characteristics of the device. In dielectric or supercapacitor applications, the appropriate formulation should preferably be identified from charging/discharging data, relaxation tails, impedance or frequency-response measurements, and agreement in amplitude and phase, rather than solely from visual comparison of time-domain responses.

2.3. Mittag–Leffler functions

The Mittag–Leffler function plays a fundamental role in the analytical representation of fractional relaxation and oscillatory electrical responses.

Definition 2.7. *For $\mu, \nu \in \mathbb{C}$ satisfying*

$$\Re(\mu) > 0, \qquad \Re(\nu) > 0,$$

the generalized Mittag–Leffler function is defined by

$$E_{\mu,\nu}(z) = \sum_{k=0}^{\infty} \frac{z^k}{\Gamma(\mu k + \nu)}. \tag{2.11}$$

The one-parameter Mittag–Leffler function is obtained as

$$E_\mu(z) = E_{\mu,1}(z).$$

Its Laplace transform satisfies

$$\mathcal{L}\left\{\tau^{\nu-1} E_{\mu,\nu}(a\tau^\mu)\right\} = \frac{s^{\mu-\nu}}{s^\mu - a}, \qquad \Re(s) > |a|^{1/\mu}. \tag{2.12}$$

2.4. Fractional-order PID controller

To improve the transient stability and damping behavior of the proposed electrical systems, a fractional–order proportional–integral–derivative (PID) controller is incorporated into the mathematical models. The transfer function of the fractional-order controller is defined by

$$C(s) = K_p + K_i s^{-\lambda} + K_d s^{\eta}, \tag{2.13}$$

where K_p, K_i, and K_d represent the proportional, integral, and derivative gains, respectively, and $\lambda, \eta \in (0, 1]$ denote the fractional integral and derivative orders. The transfer function form provides the general fractional controller representation; the specific time domain realization employed in the numerical experiments is described in Section 5. The corresponding control signal is given by

$$\mathcal{U}(\tau) = K_p e(\tau) + K_i\, {}_0\mathcal{I}_\tau^{\lambda} e(\tau) + K_d\, {}_0\mathcal{D}_\tau^{\eta} e(\tau), \tag{2.14}$$

where

$$e(\tau) = V_r(\tau) - V(\tau), \tag{2.15}$$

corresponds to the tracking error between the reference signal $V_r(\tau)$ and the system response $V(\tau)$. The inclusion of the fractional-order controller provides improved damping, suppression of oscillatory amplitudes, reduction of overshoot, and faster convergence toward the equilibrium states.

2.5. Uncertainty quantification framework

To investigate the robustness of the proposed electrical systems under parameter variability, uncertain electrical parameters are modeled probabilistically. The uncertain resistance, capacitance, and inductance are represented as

$$\mathcal{R}^* = \bar{\mathcal{R}}(1 + \varepsilon_{\mathcal{R}}), \qquad C^* = \bar{C}(1 + \varepsilon_C), \qquad \mathcal{L}^* = \bar{\mathcal{L}}(1 + \varepsilon_{\mathcal{L}}), \tag{2.16}$$

where

$$\varepsilon_{\mathcal{R}} \sim \mathcal{N}(0, \sigma_{\mathcal{R}}^2), \qquad \varepsilon_C \sim \mathcal{N}(0, \sigma_C^2), \qquad \varepsilon_{\mathcal{L}} \sim \mathcal{N}(0, \sigma_{\mathcal{L}}^2),$$

are Gaussian random perturbations. Similarly, the uncertain fractional order is modeled as

$$\vartheta^* = \bar{\vartheta} + \sigma_{\vartheta} \xi_{\vartheta}, \qquad \xi_{\vartheta} \sim \mathcal{N}(0, 1), \tag{2.17}$$

where $\bar{\vartheta}$ denotes the nominal fractional order, and σ_{ϑ} determines the magnitude of its uncertainty. For N_s Monte Carlo realizations, the sample mean and sample variance of a stochastic response Y are computed as

$$\mathbb{E}[Y] = \frac{1}{N_s} \sum_{j=1}^{N_s} Y_j, \tag{2.18}$$

and

$$\mathrm{Var}(Y) = \frac{1}{N_s - 1} \sum_{j=1}^{N_s} \left(Y_j - \mathbb{E}[Y] \right)^2. \tag{2.19}$$

To characterize the dispersion of the Monte Carlo responses without assuming a symmetric response distribution, percentile-based lower and upper uncertainty bounds are employed. Specifically,

$$Y_{\text{low}} = \mathrm{Prctile}_{p_1} \left(Y_1, \ldots, Y_{N_s} \right), \qquad Y_{\text{high}} = \mathrm{Prctile}_{p_2} \left(Y_1, \ldots, Y_{N_s} \right), \tag{2.20}$$

where p_1 and p_2 denote the selected lower and upper percentile levels, respectively. In the numerical simulations, the corresponding percentile levels are chosen consistently with the uncertainty bands reported for each experiment. The resulting percentile-based uncertainty bands provide quantitative information regarding stochastic robustness and uncertainty propagation of the proposed controlled fractional electrical systems under the considered parameter perturbations.

3. Fractional electrical circuit models with control and uncertainty

In this section, generalized fractional RC and RLC electrical circuit models with fractional-order control and uncertainty effects are formulated. The proposed models provide a unified mathematical framework for analyzing memory-dependent damping, anomalous relaxation, oscillatory suppression, and stochastic robustness in electrical systems.

3.1. Generalized fractional RC circuit

Consider a series RC electrical circuit consisting of a resistor $\mathcal{R}$ and a capacitor C connected to an external voltage source $\mathcal{E}(\tau)$. By Kirchhoff's voltage law, the classical RC circuit is governed by

$$\mathcal{R}C\frac{dV(\tau)}{d\tau} + V(\tau) = \mathcal{E}(\tau), \tag{3.1}$$

where $V(\tau)$ denotes the capacitor voltage. To preserve dimensional consistency when replacing the first-order time derivative by a fractional derivative of order ϑ, we introduce a characteristic time-scaling parameter σ_0, with dimensions of time, through

$$\frac{d}{d\tau} \longrightarrow \frac{1}{\sigma_0^{1-\vartheta}}\mathscr{D}_\tau^{(\mathcal{K},\vartheta)}. \tag{3.2}$$

Accordingly, the generalized fractional RC model can be written as

$$\mathscr{D}_\tau^{(\mathcal{K},\vartheta)}V(\tau) + \kappa_\vartheta V(\tau) = \kappa_\vartheta \mathcal{E}(\tau), \qquad 0 < \vartheta \leq 1, \tag{3.3}$$

where

$$\kappa_\vartheta = \frac{\sigma_0^{1-\vartheta}}{\mathcal{R}C} \tag{3.4}$$

is the dimensionally consistent fractional relaxation coefficient. Because $\mathcal{R}C = \mathrm{T}$, and $\sigma_0 = \mathrm{T}$, it follows that $\kappa_\vartheta = \mathrm{T}^{-\vartheta}$, consistent with the fractional derivative of order ϑ. Moreover, for $\vartheta = 1$, the scaling factor becomes unity, and $\kappa_1 = 1/(\mathcal{R}C)$, so the classical RC model is recovered. Here, $\mathscr{D}_\tau^{(\mathcal{K},\vartheta)}$ denotes the generalized fractional operator associated with the selected memory kernel $\mathcal{K}$. The generalized Laplace domain representation of (3.3) is given by

$$[\mathcal{K}_\vartheta(s) + \kappa_\vartheta]\,\widehat{V}(s) = \mathcal{I}_\vartheta(s) + \kappa_\vartheta\widehat{\mathcal{E}}(s), \tag{3.5}$$

where $\mathcal{K}_\vartheta(s)$ denotes the Laplace symbol of the selected fractional operator and $\mathcal{I}_\vartheta(s)$ contains the initial condition contributions. The corresponding analytical solution is expressed as

$$V(\tau) = V_0\mathcal{G}_\vartheta(\tau) + \kappa_\vartheta \int_0^\tau \mathcal{G}_\vartheta(\tau-\xi)\mathcal{E}(\xi)\,d\xi, \tag{3.6}$$

where $\mathcal{G}_\vartheta(\tau)$ denotes the relaxation kernel associated with the selected fractional operator. Its structure determines the dynamics, including power law memory, exponential stabilization, Mittag–Leffler crossover behavior, or localized conformable scaling.

3.2. Controlled fractional RC circuit

To improve the transient performance of the fractional RC system, a fractional-order control input is incorporated into the governing model. The controlled fractional RC circuit is written as

$$\mathscr{D}_{\tau}^{(\mathcal{K},\vartheta)}V(\tau) + \kappa_{\vartheta}V(\tau) + \mathcal{U}(\tau) = \kappa_{\vartheta}\mathcal{E}(\tau), \tag{3.7}$$

where the control signal is defined by

$$\mathcal{U}(\tau) = K_p e(\tau) + K_i\, {}_0\mathcal{I}_{\tau}^{\lambda} e(\tau) + K_d\, {}_0\mathcal{D}_{\tau}^{\eta} e(\tau), \tag{3.8}$$

with

$$e(\tau) = V_r(\tau) - V(\tau). \tag{3.9}$$

Taking the Laplace transform gives

$$\left[\mathcal{K}_{\vartheta}(s) + \kappa_{\vartheta} + K_p + K_i s^{-\lambda} + K_d s^{\eta}\right]\widehat{V}(s) = \mathcal{I}_{\vartheta}(s) + \kappa_{\vartheta}\widehat{\mathcal{E}}(s) + \left[K_p + K_i s^{-\lambda} + K_d s^{\eta}\right]\widehat{V}_r(s). \tag{3.10}$$

For zero reference input, the controlled transfer function becomes

$$G_{RC}^{c}(s) = \frac{\widehat{V}(s)}{\widehat{\mathcal{E}}(s)} = \frac{\kappa_{\vartheta}}{\mathcal{K}_{\vartheta}(s) + \kappa_{\vartheta} + K_p + K_i s^{-\lambda} + K_d s^{\eta}}. \tag{3.11}$$

The fractional-order controller improves damping behavior, suppresses oscillatory amplitudes, and enhances asymptotic convergence of the electrical response.

3.3. Uncertain fractional RC circuit

To model stochastic variability arising from manufacturing tolerances, thermal fluctuations, and environmental perturbations, the uncertain electrical parameters are introduced as

$$\mathcal{R}^* = \bar{\mathcal{R}}(1 + \varepsilon_{\mathcal{R}}), \qquad C^* = \bar{C}(1 + \varepsilon_C), \tag{3.12}$$

where

$$\varepsilon_{\mathcal{R}} \sim \mathcal{N}(0, \sigma_{\mathcal{R}}^2), \qquad \varepsilon_C \sim \mathcal{N}(0, \sigma_C^2).$$

The uncertain fractional order is represented by

$$\vartheta^* = \bar{\vartheta} + \sigma_{\vartheta}\xi_{\vartheta}, \qquad \xi_{\vartheta} \sim \mathcal{N}(0, 1), \tag{3.13}$$

where $\bar{\vartheta}$ denotes the nominal fractional order, and σ_{ϑ} determines the magnitude of its uncertainty. Consequently, the uncertain fractional relaxation coefficient becomes

$$\kappa_{\vartheta^*}^* = \frac{\sigma_0^{1-\vartheta^*}}{\mathcal{R}^* C^*}, \tag{3.14}$$

where σ_0 is the same characteristic time-scaling parameter introduced in the deterministic fractional RC model. The uncertain controlled RC model is therefore written as

$$\mathscr{D}_{\tau}^{(\mathcal{K},\vartheta^*)}V^*(\tau) + \kappa_{\vartheta^*}^* V^*(\tau) + \mathcal{U}^*(\tau) = \kappa_{\vartheta^*}^*\mathcal{E}(\tau). \tag{3.15}$$

3.4. Generalized fractional RLC circuit

Consider a series RLC electrical circuit consisting of a resistor $\mathcal{R}$, an inductor $\mathcal{L}$, and a capacitor C connected to an external voltage source $\mathcal{E}(\tau)$. The classical RLC circuit is governed by

$$\mathcal{L}\frac{d^2Q(\tau)}{d\tau^2} + \mathcal{R}\frac{dQ(\tau)}{d\tau} + \frac{1}{C}Q(\tau) = \mathcal{E}(\tau), \tag{3.16}$$

where $Q(\tau)$ denotes the capacitor charge. To preserve dimensional consistency in the fractional-order formulation, the first- and second-order temporal derivatives are replaced according to

$$\frac{d}{d\tau} \longrightarrow \frac{1}{\sigma_0^{1-\vartheta}}\mathscr{D}_\tau^{(\mathcal{K},\vartheta)}, \qquad \frac{d^2}{d\tau^2} \longrightarrow \frac{1}{\sigma_0^{2(1-\vartheta)}}\mathscr{D}_\tau^{(\mathcal{K},2\vartheta)}, \tag{3.17}$$

where σ_0 is a characteristic time-scaling parameter with dimensions of time. Accordingly, the generalized fractional RLC model is formulated as

$$\mathscr{D}_\tau^{(\mathcal{K},2\vartheta)}Q(\tau) + a_\vartheta\mathscr{D}_\tau^{(\mathcal{K},\vartheta)}Q(\tau) + b_\vartheta Q(\tau) = b_\vartheta C\mathcal{E}(\tau), \tag{3.18}$$

where

$$a_\vartheta = \frac{\mathcal{R}}{\mathcal{L}}\sigma_0^{1-\vartheta}, \qquad b_\vartheta = \frac{\sigma_0^{2(1-\vartheta)}}{\mathcal{L}C}. \tag{3.19}$$

Because $\mathcal{R}/\mathcal{L} = \mathrm{T}^{-1}$, $\mathcal{L}C = \mathrm{T}^2$, and $\sigma_0 = \mathrm{T}$, the coefficients a_ϑ and b_ϑ have dimensions $\mathrm{T}^{-\vartheta}$ and $\mathrm{T}^{-2\vartheta}$, respectively. For $\vartheta = 1$, the scaling factors reduce automatically to unity, giving $a_1 = \mathcal{R}/\mathcal{L}$ and $b_1 = 1/(\mathcal{L}C)$, and hence recovering the classical RLC formulation. The corresponding Laplace domain representation is

$$[\mathcal{K}_{2\vartheta}(s) + a_\vartheta\mathcal{K}_\vartheta(s) + b_\vartheta]\,\widehat{Q}(s) = \mathcal{J}_\vartheta(s) + b_\vartheta C\widehat{\mathcal{E}}(s), \tag{3.20}$$

where $\mathcal{J}_\vartheta(s)$ contains the initial condition contributions. The proposed generalized fractional RLC framework captures memory-dependent oscillatory behavior, anomalous damping mechanisms, fractional relaxation effects, and hereditary energy dissipation dynamics. Accordingly, the uncertain fractional coefficients are defined as

$$a^*_{\vartheta^*} = \frac{\mathcal{R}^*}{\mathcal{L}^*}\sigma_0^{1-\vartheta^*}, \qquad b^*_{\vartheta^*} = \frac{\sigma_0^{2(1-\vartheta^*)}}{\mathcal{L}^*C^*}. \tag{3.21}$$

These coefficients account for both the uncertain electrical parameters and the uncertain fractional order while preserving dimensional consistency. The resulting uncertain controlled fractional RLC system is written as

$$\mathscr{D}_\tau^{(\mathcal{K},2\vartheta^*)}Q^*(\tau) + a^*_{\vartheta^*}\mathscr{D}_\tau^{(\mathcal{K},\vartheta^*)}Q^*(\tau) + b^*_{\vartheta^*}Q^*(\tau) + \mathcal{U}^*_Q(\tau) = b^*_{\vartheta^*}C^*\mathcal{E}(\tau). \tag{3.22}$$

The generalized fractional electrical models exhibit distinct dynamics depending on the memory kernel and fractional order. Lower fractional orders enhance hereditary effects and slow relaxation; singular power law kernels produce long-tail memory, and nonsingular kernels yield smoother stabilization. Fractional-order control improves damping, reduces oscillations, and enhances transient stability in RC and RLC systems. The uncertainty framework further quantifies stochastic robustness to parameter perturbations through mean responses and uncertainty bands.

3.5. Stability, damping, and frequency response characteristics

The stability and dynamical behavior of the fractional RC and RLC models can be characterized through their Laplace domain operators. For the generalized RC circuit, the characteristic relation is

$$\mathcal{K}_\vartheta(s) + \kappa_\vartheta = 0, \tag{3.23}$$

where $\mathcal{K}_\vartheta(s)$ denotes the Laplace symbol of the selected fractional operator. For the Liouville–Caputo case, $\mathcal{K}_\vartheta(s) = s^\vartheta$, and the homogeneous response is proportional to $E_\vartheta(-\kappa_\vartheta \tau^\vartheta)$. For $0 < \vartheta \leq 1$ and $\kappa_\vartheta > 0$, this response decays asymptotically. For $\vartheta < 1$, the Mittag–Leffler relaxation exhibits a longer memory tail than the exponential relaxation recovered at $\vartheta = 1$. For the Liouville–Caputo RLC model, the modal behavior follows from the characteristic equation derived in the analytical solution. The transformed roots determine whether the response is oscillatory or nonoscillatory, whereas asymptotic stability of the corresponding commensurate fractional system is governed by

$$\left|\arg(\lambda_j)\right| > \frac{\vartheta\pi}{2}, \tag{3.24}$$

where λ_j denotes a modal eigenvalue. This condition is the fractional counterpart of the classical left-half-plane stability criterion. Thus, the fractional order together with the coefficients a_ϑ and b_ϑ determines the decay and oscillatory characteristics of the RLC response. The frequency response further reveals the influence of the memory kernel. For harmonic excitation of angular frequency ω, the generalized RC and RLC frequency response functions can be written as

$$G_{\mathrm{RC}}(i\omega) = \frac{\kappa_\vartheta}{\mathcal{K}_\vartheta(i\omega) + \kappa_\vartheta}, \qquad G_{\mathrm{RLC}}(i\omega) = \frac{b_\vartheta C}{\mathcal{K}_{2\vartheta}(i\omega) + a_\vartheta \mathcal{K}_\vartheta(i\omega) + b_\vartheta}. \tag{3.25}$$

The corresponding amplitude and phase responses are determined by $|G(i\omega)|$ and $\arg G(i\omega)$, respectively. Because $\mathcal{K}_\vartheta(i\omega)$ depends on the selected fractional operator, different memory kernels produce different attenuation and phase characteristics under periodic excitation. For the Liouville–Caputo operator

$$(i\omega)^\vartheta = \omega^\vartheta \exp\left(i\frac{\pi\vartheta}{2}\right),$$

which explicitly demonstrates the dependence of the frequency response on the fractional order, the classical integer-order models are recovered at $\vartheta = 1$, for which $\mathcal{K}_1(s) = s$, and $\mathcal{K}_2(s) = s^2$. The RC circuit then exhibits the usual exponential relaxation, whereas the classical RLC circuit has

$$\omega_n = \frac{1}{\sqrt{\mathcal{L}C}}, \qquad \zeta = \frac{\mathcal{R}}{2}\sqrt{\frac{C}{\mathcal{L}}},$$

where ω_n and ζ are the natural frequency and damping ratio, respectively. For $\vartheta < 1$, the fractional order and memory kernel introduce additional frequency-dependent attenuation, phase shift, and nonexponential relaxation. The integer-order model therefore provides a reference for quantifying the memory-dependent changes in damping, relaxation, and oscillatory behavior.

4. Analytical solutions of the proposed fractional circuit models

In this section, analytical solutions of the proposed generalized fractional RC and RLC circuit models are derived. The Laplace transform method, convolution theorem, Mittag–Leffler functions, and transfer-function representations are employed to obtain explicit solution formulas under constant and periodic excitations. The effects of fractional–order control and uncertainty propagation are also incorporated into the analytical framework. Before deriving the operator-specific solutions, we note the basic well-posedness of the analytical representations used below. For $\Re(\mu) > 0$, the generalized Mittag–Leffler function

$$E_{\mu,\nu}(z) = \sum_{k=0}^{\infty} \frac{z^k}{\Gamma(\mu k + \nu)}$$

is an entire function of z, and therefore, its defining series converges absolutely for every finite z. Consequently, the Mittag–Leffler kernels appearing in the RC and RLC solutions are continuous on finite time intervals, apart from the integrable weak singularities explicitly associated with the Caputo-type kernels. For continuous forcing and admissible initial data, the resulting convolution integrals are therefore well–defined. Moreover, the Laplace domain solution has the generic form

$$\widehat{Y}(s) = \frac{\mathcal{I}(s) + \mathcal{F}(s)}{\Delta(s)},$$

where $\Delta(s)$ is the characteristic function of the selected fractional operator. Whenever $\Delta(s)$ has no zeros in the admissible Laplace half-plane, inversion of the Laplace transform yields a unique solution. Indeed, the difference of any two solutions satisfying the same initial data has a vanishing Laplace transform and therefore vanishes identically. These properties justify the Mittag–Leffler and convolution representations used in the following analytical derivations.

4.1. Analytical solution of the fractional RC circuit

Consider the generalized fractional RC circuit

$$\mathscr{D}_{\tau}^{(\mathcal{K},\vartheta)} V(\tau) + \kappa_{\vartheta} V(\tau) = \kappa_{\vartheta} \mathcal{E}(\tau), \qquad 0 < \vartheta \leq 1, \tag{4.1}$$

with initial condition

$$V(0) = V_0, \tag{4.2}$$

where

$$\kappa_{\vartheta} = \frac{\sigma_0^{1-\vartheta}}{\mathcal{R}C} \tag{4.3}$$

is the dimensionally consistent fractional relaxation coefficient, with σ_0 denoting the characteristic time-scaling parameter introduced previously. Because $[\sigma_0]$ = time, and $[\mathcal{R}C]$ = time, it follows that $[\kappa_{\vartheta}] = \text{time}^{-\vartheta}$, which is consistent with the fractional derivative of order ϑ. Moreover, for $\vartheta = 1$, the classical relaxation coefficient $\kappa_1 = 1/(\mathcal{R}C)$ is recovered automatically. Applying the Laplace transform to (4.1) gives

$$[\mathcal{K}_{\vartheta}(s) + \kappa_{\vartheta}]\, \widehat{V}(s) = \mathcal{I}_{\vartheta}(s) + \kappa_{\vartheta} \widehat{\mathcal{E}}(s), \tag{4.4}$$

where $\mathcal{K}_{\vartheta}(s)$ denotes the Laplace symbol of the selected fractional operator, and $\mathcal{I}_{\vartheta}(s)$ contains the initial condition terms.

4.1.1. Nonsingular memory kernels

For nonsingular memory kernels such as the Caputo–Fabrizio, Atangana–Baleanu, and Atangana–Koca operators, the analytical solutions retain a generalized convolution structure, and the corresponding relaxation behavior is determined by the Laplace symbol of the selected fractional operator. The dimensionally consistent fractional relaxation coefficient is

$$\kappa_\vartheta = \frac{\sigma_0^{1-\vartheta}}{\mathcal{R}C}, \tag{4.5}$$

where σ_0 is the characteristic time-scaling parameter introduced previously.

For the Caputo–Fabrizio operator, define

$$A_{\mathrm{CF}} = \mathcal{N}(\vartheta) + \kappa_\vartheta(1-\vartheta), \qquad \lambda_{\mathrm{CF}} = \frac{\vartheta\kappa_\vartheta}{A_{\mathrm{CF}}}. \tag{4.6}$$

The corresponding relaxation kernel is

$$\mathcal{G}_\vartheta^{\mathrm{CF}}(\tau) = \frac{\mathcal{N}(\vartheta)}{A_{\mathrm{CF}}} \exp\left(-\lambda_{\mathrm{CF}}\tau\right). \tag{4.7}$$

Hence, for constant excitation $\mathcal{E}(\tau) = E_0$, the response can be represented as

$$V_{\mathrm{CF}}(\tau) = V_0\mathcal{G}_\vartheta^{\mathrm{CF}}(\tau) + \kappa_\vartheta E_0 \int_0^\tau \mathcal{G}_\vartheta^{\mathrm{CF}}(\tau-\xi)\, d\xi. \tag{4.8}$$

For the periodic excitation $\mathcal{E}(\tau) = E_0 \sin(\omega\tau)$, the Caputo–Fabrizio response is explicitly written as

$$\begin{aligned} V_{\mathrm{CF}}(\tau) = {} & \frac{\mathcal{N}(\vartheta)}{A_{\mathrm{CF}}} V_0 e^{-\lambda_{\mathrm{CF}}\tau} + \frac{\kappa_\vartheta(1-\vartheta)}{A_{\mathrm{CF}}} E_0 \sin(\omega\tau) \\ & + \frac{\kappa_\vartheta\vartheta\mathcal{N}(\vartheta)}{A_{\mathrm{CF}}^2} E_0 \int_0^\tau e^{-\lambda_{\mathrm{CF}}(\tau-\xi)} \sin(\omega\xi)\, d\xi. \end{aligned} \tag{4.9}$$

Thus, the periodic response consists of a decaying initial condition contribution, a direct forcing contribution, and an exponentially weighted convolution term representing the nonsingular memory effect.

Similarly, for the Atangana–Baleanu operator, define

$$A_{\mathrm{AB}} = \mathcal{B}(\vartheta) + \kappa_\vartheta(1-\vartheta), \qquad \lambda_{\mathrm{AB}} = \frac{\vartheta\kappa_\vartheta}{A_{\mathrm{AB}}}. \tag{4.10}$$

The corresponding relaxation kernel is

$$\mathcal{G}_\vartheta^{\mathrm{AB}}(\tau) = \frac{\mathcal{B}(\vartheta)}{A_{\mathrm{AB}}} E_\vartheta\left(-\lambda_{\mathrm{AB}}\tau^\vartheta\right). \tag{4.11}$$

For constant excitation $\mathcal{E}(\tau) = E_0$, the response is represented as

$$V_{\mathrm{AB}}(\tau) = V_0\mathcal{G}_\vartheta^{\mathrm{AB}}(\tau) + \kappa_\vartheta E_0 \int_0^\tau \mathcal{G}_\vartheta^{\mathrm{AB}}(\tau-\xi)\, d\xi. \tag{4.12}$$

For the periodic excitation $\mathcal{E}(\tau) = E_0 \sin(\omega\tau)$, the Atangana–Baleanu response is explicitly given by

$$\begin{aligned} V_{\mathrm{AB}}(\tau) = {} & \frac{\mathcal{B}(\vartheta)}{A_{\mathrm{AB}}} V_0 E_\vartheta\left(-\lambda_{\mathrm{AB}}\tau^\vartheta\right) + \frac{\kappa_\vartheta(1-\vartheta)}{A_{\mathrm{AB}}} E_0 \sin(\omega\tau) \\ & + \frac{\kappa_\vartheta \vartheta \mathcal{B}(\vartheta)}{A_{\mathrm{AB}}^2} E_0 \int_0^\tau (\tau-\xi)^{\vartheta-1} E_{\vartheta,\vartheta}\left(-\lambda_{\mathrm{AB}}(\tau-\xi)^\vartheta\right) \sin(\omega\xi)\, d\xi. \end{aligned} \tag{4.13}$$

The last integral represents the convolution of the periodic forcing with the Mittag–Leffler memory kernel. For the Atangana–Koca operator, introduce the generalized Mittag–Leffler kernel

$$\Phi_\vartheta(\tau) = E_{\vartheta,\vartheta}^{\vartheta}\left(-\chi(\vartheta)\tau^\vartheta\right). \tag{4.14}$$

Using the series definition of the three-parameter, generalized Mittag–Leffler function and applying the Laplace transform term by term gives

$$\widehat{\Phi}_\vartheta(s) = \sum_{k=0}^{\infty} \frac{(\vartheta)_k[-\chi(\vartheta)]^k \Gamma(\vartheta k+1)}{k!\,\Gamma(\vartheta k+\vartheta)} s^{-(\vartheta k+1)}. \tag{4.15}$$

Consequently, the Laplace transform of the Atangana–Koca derivative defined in (2.7) is

$$\mathcal{L}\left\{{}^{\mathrm{AK}}\mathcal{D}_\tau^\vartheta \psi(\tau)\right\} = \frac{\widehat{\Phi}_\vartheta(s)}{\chi(\vartheta)} \left[s\Psi(s) - \psi(0)\right]. \tag{4.16}$$

Therefore, the Laplace domain symbol associated with the Atangana–Koca operator is

$$\mathcal{K}_\vartheta^{\mathrm{AK}}(s) = \frac{s\,\widehat{\Phi}_\vartheta(s)}{\chi(\vartheta)}, \tag{4.17}$$

with the corresponding initial condition contribution

$$\mathcal{I}_\vartheta^{\mathrm{AK}}(s) = \frac{V_0 \widehat{\Phi}_\vartheta(s)}{\chi(\vartheta)}. \tag{4.18}$$

Substitution into (4.4) yields

$$\widehat{V}_{\mathrm{AK}}(s) = V_0 \frac{\widehat{\Phi}_\vartheta(s)}{s\widehat{\Phi}_\vartheta(s) + \kappa_\vartheta\chi(\vartheta)} + \kappa_\vartheta \frac{\chi(\vartheta)}{s\widehat{\Phi}_\vartheta(s) + \kappa_\vartheta\chi(\vartheta)} \widehat{\mathcal{E}}(s). \tag{4.19}$$

Accordingly, the Atangana–Koca relaxation kernel is

$$\mathcal{G}_\vartheta^{\mathrm{AK}}(\tau) = \mathcal{L}^{-1}\left\{\frac{\widehat{\Phi}_\vartheta(s)}{s\widehat{\Phi}_\vartheta(s) + \kappa_\vartheta\chi(\vartheta)}\right\}(\tau), \tag{4.20}$$

and the corresponding forcing kernel is

$$\mathcal{H}_\vartheta^{\mathrm{AK}}(\tau) = \mathcal{L}^{-1}\left\{\frac{\chi(\vartheta)}{s\widehat{\Phi}_\vartheta(s) + \kappa_\vartheta\chi(\vartheta)}\right\}(\tau). \tag{4.21}$$

Thus, for the periodic excitation $\mathcal{E}(\tau) = E_0 \sin(\omega\tau)$, the Atangana–Koca response is

$$V_{\mathrm{AK}}(\tau) = V_0 \mathcal{G}_\vartheta^{\mathrm{AK}}(\tau) + \kappa_\vartheta E_0 \int_0^\tau \mathcal{H}_\vartheta^{\mathrm{AK}}(\tau-\xi) \sin(\omega\xi)\, d\xi. \tag{4.22}$$

This formulation explicitly identifies the Laplace domain symbol, relaxation kernel, forcing kernel, and periodic convolution structure of the Atangana–Koca model and is consistent with the generalized Mittag–Leffler kernel adopted in Definition 2.4.

4.2. Controlled fractional RC circuit

The controlled fractional RC circuit is governed by

$$\mathscr{D}_{\tau}^{(\mathcal{K},\vartheta)}V(\tau) + \kappa_{\vartheta}V(\tau) + \mathcal{U}(\tau) = \kappa_{\vartheta}\mathcal{E}(\tau), \tag{4.23}$$

where

$$\kappa_{\vartheta} = \frac{\sigma_0^{1-\vartheta}}{\mathcal{R}C} \tag{4.24}$$

is the dimensionally consistent fractional relaxation coefficient introduced previously, and the control signal is defined by

$$\mathcal{U}(\tau) = K_p e(\tau) + K_i\, {}_0\mathcal{I}_{\tau}^{\lambda}e(\tau) + K_d\, {}_0\mathcal{D}_{\tau}^{\eta}e(\tau), \tag{4.25}$$

with

$$e(\tau) = V_r(\tau) - V(\tau).$$

Taking the Laplace transform yields

$$\left[\mathcal{K}_{\vartheta}(s) + \kappa_{\vartheta} + K_p + K_i s^{-\lambda} + K_d s^{\eta}\right]\widehat{V}(s) = \mathcal{I}_{\vartheta}(s) + \kappa_{\vartheta}\widehat{\mathcal{E}}(s) + \left[K_p + K_i s^{-\lambda} + K_d s^{\eta}\right]\widehat{V}_r(s). \tag{4.26}$$

For zero reference input, the transfer function becomes

$$G_{RC}^{c}(s) = \frac{\widehat{V}(s)}{\widehat{\mathcal{E}}(s)} = \frac{\kappa_{\vartheta}}{\mathcal{K}_{\vartheta}(s) + \kappa_{\vartheta} + K_p + K_i s^{-\lambda} + K_d s^{\eta}}. \tag{4.27}$$

The fractional-order controller significantly improves damping behavior, suppresses oscillatory amplitudes, and accelerates convergence toward equilibrium states.

4.3. Analytical solution of the fractional RLC circuit

The generalized fractional RLC circuit is modeled by

$$\mathscr{D}_{\tau}^{(\mathcal{K},2\vartheta)}Q(\tau) + a_{\vartheta}\mathscr{D}_{\tau}^{(\mathcal{K},\vartheta)}Q(\tau) + b_{\vartheta}Q(\tau) = b_{\vartheta}C\mathcal{E}(\tau), \tag{4.28}$$

where

$$a_{\vartheta} = \frac{\mathcal{R}}{\mathcal{L}}\sigma_0^{1-\vartheta}, \qquad b_{\vartheta} = \frac{\sigma_0^{2(1-\vartheta)}}{\mathcal{L}C}. \tag{4.29}$$

Here, σ_0 is the characteristic time-scaling parameter introduced previously to preserve dimensional consistency in the fractional-order formulation. Accordingly, a_{ϑ} and b_{ϑ} have dimensions of time$^{-\vartheta}$ and time$^{-2\vartheta}$, respectively. Moreover, for $\vartheta = 1$, the classical coefficients $a_1 = \mathcal{R}/\mathcal{L}$ and $b_1 = 1/(\mathcal{L}C)$ are recovered automatically. Applying the Laplace transform gives

$$\widehat{Q}(s) = \frac{\mathcal{J}_{\vartheta}(s) + b_{\vartheta}C\widehat{\mathcal{E}}(s)}{\mathcal{K}_{2\vartheta}(s) + a_{\vartheta}\mathcal{K}_{\vartheta}(s) + b_{\vartheta}}, \tag{4.30}$$

where $\mathcal{J}_{\vartheta}(s)$ contains the initial condition contributions. For the Caputo kernel,

$$\mathcal{K}_{\vartheta}(s) = s^{\vartheta}, \qquad \mathcal{K}_{2\vartheta}(s) = s^{2\vartheta},$$

the homogeneous solution is

$$Q_h(\tau) = C_1 E_\vartheta \left(z_1 \tau^\vartheta\right) + C_2 E_\vartheta \left(z_2 \tau^\vartheta\right), \tag{4.31}$$

and the periodic forced response is represented by

$$Q_p(\tau) = b_\vartheta C E_0 \int_0^\tau G_{RLC}(\xi) \sin\left(\omega(\tau - \xi)\right) \, d\xi, \tag{4.32}$$

where

$$G_{RLC}(\tau) = \mathcal{L}^{-1}\left\{\frac{1}{s^{2\vartheta} + a_\vartheta s^\vartheta + b_\vartheta}\right\} \tag{4.33}$$

denotes the fractional impulse response. The resulting analytical solutions capture memory-dependent oscillatory dynamics, anomalous damping behavior, and hereditary energy dissipation mechanisms in fractional RLC systems.

4.4. Controlled fractional RLC circuit

The controlled fractional RLC system is written as

$$\mathscr{D}_\tau^{(\mathcal{K},2\vartheta)} Q(\tau) + a_\vartheta \mathscr{D}_\tau^{(\mathcal{K},\vartheta)} Q(\tau) + b_\vartheta Q(\tau) + \mathcal{U}_Q(\tau) = b_\vartheta C \mathcal{E}(\tau), \tag{4.34}$$

where the dimensionally consistent fractional coefficients are

$$a_\vartheta = \frac{\mathcal{R}}{\mathcal{L}} \sigma_0^{1-\vartheta}, \qquad b_\vartheta = \frac{\sigma_0^{2(1-\vartheta)}}{\mathcal{L}C}, \tag{4.35}$$

with σ_0 denoting the characteristic time-scaling parameter introduced previously. Accordingly, a_ϑ and b_ϑ have dimensions of time$^{-\vartheta}$ and time$^{-2\vartheta}$, respectively. For $\vartheta = 1$, the classical coefficients $a_1 = \mathcal{R}/\mathcal{L}$ and $b_1 = 1/(\mathcal{L}C)$ are recovered automatically. The control signal is defined by

$$\mathcal{U}_Q(\tau) = K_p e_Q(\tau) + K_i \, {}_0\mathcal{I}_\tau^\lambda e_Q(\tau) + K_d \, {}_0\mathcal{D}_\tau^\eta e_Q(\tau), \tag{4.36}$$

with

$$e_Q(\tau) = Q_r(\tau) - Q(\tau). \tag{4.37}$$

For zero reference input, the transfer function becomes

$$G_{RLC}^c(s) = \frac{b_\vartheta C}{\mathcal{K}_{2\vartheta}(s) + a_\vartheta \mathcal{K}_\vartheta(s) + b_\vartheta + K_p + K_i s^{-\lambda} + K_d s^\eta}. \tag{4.38}$$

The fractional-order controller improves transient stability, suppresses oscillatory responses, and enhances damping efficiency in the fractional RLC system.

4.5. Uncertainty propagation

Let

$$\Theta = \left(\mathcal{R}, C, \mathcal{L}, \vartheta, K_p, K_i, K_d\right) \tag{4.39}$$

denote the uncertain parameter vector. The stochastic system response is represented by

$$Y(\tau, \Theta) = \begin{cases} V(\tau, \Theta), & \text{for RC circuits,} \\ Q(\tau, \Theta), & \text{for RLC circuits.} \end{cases} \tag{4.40}$$

The present uncertainty analysis considers Gaussian-distributed parameter perturbations as a controlled stochastic model of component and model variability. These perturbations should not be interpreted as a complete representation of practical circuit disturbances. In physical circuits, manufacturing tolerances may follow bounded non-Gaussian distributions, thermal effects may introduce slowly time-varying parameter drift, and electromagnetic interference may generate impulsive disturbances. For N_s Monte Carlo realizations, the corresponding responses are

$$Y_j(\tau) = Y(\tau, \Theta_j), \qquad j = 1, 2, \ldots, N_s. \tag{4.41}$$

The sample mean and variance are computed by

$$\mathbb{E}[Y(\tau)] = \frac{1}{N_s} \sum_{j=1}^{N_s} Y_j(\tau), \tag{4.42}$$

and

$$\mathrm{Var}[Y(\tau)] = \frac{1}{N_s - 1} \sum_{j=1}^{N_s} \Big[Y_j(\tau) - \mathbb{E}[Y(\tau)] \Big]^2 . \tag{4.43}$$

To characterize the dispersion of the Monte Carlo responses without assuming a symmetric response distribution, the lower and upper percentile-based uncertainty bounds are defined as

$$Y_{\text{low}}(\tau) = \text{Prctile}_{p_1}\left(Y_1(\tau), \ldots, Y_{N_s}(\tau)\right), \tag{4.44}$$

$$Y_{\text{high}}(\tau) = \text{Prctile}_{p_2}\left(Y_1(\tau), \ldots, Y_{N_s}(\tau)\right), \tag{4.45}$$

where p_1 and p_2 denote the selected lower and upper percentile levels, respectively. The percentile levels are chosen consistently with the uncertainty bands reported in the corresponding numerical experiments. The resulting percentile-based uncertainty bands provide quantitative information regarding stochastic robustness and uncertainty propagation of the proposed controlled fractional electrical systems under the considered parameter perturbations.

5. Results and discussion

In this section, we perform numerical simulations to explore the dynamical behavior of the proposed fractional RC and RLC electrical circuit models under different fractional operators, fractional-order control strategies, and uncertainty quantification settings. The results demonstrate the effects of fractional memory, stochastic perturbations and control parameters on transient and oscillatory responses of the studied electrical systems. Numerical computation of the Mittag–Leffler functions is carried out, and uncertainty propagation is studied by Monte Carlo simulations. The main numerical parameters, fractional-order controller parameters, levels of uncertainty, Monte Carlo sample sizes, percentile intervals, and random-number seeds used in Figures 1–6 are summarized in Table 1 for reproducibility.

Table 1. Numerical, control, and uncertainty settings used in the simulations shown in Figures 1–6.

Figure	Numerical setup	Fractional/operator parameters	Controller parameters	Uncertainty quantification
1	$t \in [0, 6]$ $N_t = 800$	$\vartheta = (0.98, 0.96, 0.94, 0.92)$ $\beta = (0.97, 0.95, 0.96, 0.95)$ $\tau_a = 1$	$K_p = 0.45,\ K_i = 0.35$ $\lambda_c = 0.85,\ K_d = 0$	$N_s = 400$ $\sigma_\vartheta = 0.020,\ \sigma_\tau = 0.075$ $\sigma_{K_p} = 0.080,\ \sigma_{K_i} = 0.060$ 10–90% band; seeds 101–104
2	$t \in [0, 6]$ $N_t = 800$	$\vartheta = (0.98, 0.96, 0.94, 0.92)$ $\beta = (0.97, 0.95, 0.96, 0.95)$ $\tau_a = 1$	$K_p = 0.45,\ K_i = 0.35$ $\lambda_c = 0.85,\ K_d = 0$	$N_s = 400$ $\sigma_\vartheta = 0.020,\ \sigma_\tau = 0.075$ $\sigma_{K_p} = 0.080,\ \sigma_{K_i} = 0.060$ 10–90% band; seeds 201–204
3	$t \in [0, 32]$ $N_t = 4000$	$\vartheta = (0.98, 0.96, 0.94, 0.92)$ $\beta = (0.97, 0.98, 0.93, 0.95)$ $A_{\text{tr}} = 0.36,\ A_{\text{ss}} = 0.09$ $\Omega = \pi$	$K_p = 0.35,\ K_i = 0.25$ $\lambda_c = 0.85,\ K_d = 0$	$N_s = 400$ $\sigma_\vartheta = 0.020,\ \sigma_d = 0.070$ $\sigma_{K_p} = 0.060,\ \sigma_{K_i} = 0.050$ 10–90% band; seeds 301–304
4	$t \in [0, 15]$ $N_t = 2500$	$\vartheta = (0.92, 0.96, 0.94, 0.98)$ $\beta = (0.95, 0.98, 0.97, 0.97)$ $A = 4.2,\ Q_{\text{ss}} = 1$	$K_p = 0.80,\ K_i = 0.65$ $\lambda_c = 0.85,\ K_d = 0$	$N_s = 300$ $\sigma_\vartheta = 0.030,\ \sigma_d = 0.120$ $\sigma_\omega = 0.080,\ \sigma_{K_p} = 0.150$ 5–95% band; seeds 401–404
5	$t \in [0, 15]$ $N_t = 2500$	$\vartheta = (0.98, 0.96, 0.94, 0.92)$ $\beta = (0.97, 0.98, 0.97, 0.95)$ $A_0 = 5.0,\ A_{\text{per}} = 0.22$ $\omega = 2.88,\ \Omega = 2.82$	$K_p = 0.80,\ K_i = 0.65$ $\lambda_c = 0.85,\ K_d = 0$	$N_s = 300$ $\sigma_\vartheta = 0.030,\ \sigma_d = 0.120$ $\sigma_\omega = 0.080,\ \sigma_A = 0.100$ $\sigma_{K_p} = 0.150$ 5–95% band; seeds 501–504
6(a)	$t \in [0, 100]$ $N_t = 2500$ $V_{\max} = 7.5,\ \tau = 10$	$\vartheta_{\text{C}} = 0.970,\ \vartheta_{\text{AB}} = 0.985$ $\vartheta_{\text{AK}} = 0.992$ FC: (0.975, 0.985) CF: 1.08τ	$K_p = 0.12,\ K_i = 0.04$ $\lambda_c = 0.85,\ K_d = 0$	$N_s = 200$ $\sigma_\tau = 0.015,\ \sigma_{K_p} = 0.015$ 25–75% band; seed 600
6(b)	$t \in [0, 100]$ $N_t = 2500$ $V_{\max} = 7.5,\ \tau = 10$	$\vartheta_{\text{C}} = 0.975,\ \vartheta_{\text{AB}} = 0.988$ $\vartheta_{\text{AK}} = 0.993$ FC: (0.980, 0.990) CF: 1.06τ	$K_p = 0.12,\ K_i = 0.04$ $\lambda_c = 0.85,\ K_d = 0$	$N_s = 200$ $\sigma_\tau = 0.015,\ \sigma_{K_p} = 0.015$ 25–75% band; seed 700

In the numerical experiments reported, the controller is implemented as a fractional PI controller, and thus, the derivative gain is set to $K_d = 0$. In the numerical implementations, the time-dependent control strength is defined as

$$C(\tau) = K_p + \frac{K_i \tau^{\lambda_c}}{\Gamma(\lambda_c + 1)}. \tag{5.1}$$

To clarify the relation between the transfer-function representation introduced in Section 2 and the numerical implementation, setting $K_d = 0$ gives the fractional PI controller

$$C_{\text{PI}}(s) = K_p + K_i s^{-\lambda_c}. \tag{5.2}$$

Using

$$\mathcal{L}^{-1}\{s^{-\lambda_c}\} = \frac{\tau^{\lambda_c-1}}{\Gamma(\lambda_c)}, \qquad {}_0I_\tau^{\lambda_c}1 = \frac{\tau^{\lambda_c}}{\Gamma(\lambda_c+1)}, \tag{5.3}$$

the normalized time domain realization of the fractional integral term leads directly to the control strength function defined in (5.1). Thus, Eq (5.1) is not an independent controller; it is the time domain fractional PI control strength realization adopted for the numerical modulation. In particular, the simulations do not numerically evaluate a separate tracking error history integral. Instead, $C(\tau)$ is evaluated pointwise at every time step and inserted directly into the controlled analytical response. For Figures 1 and 2, $C(\tau)$ modifies the effective fractional relaxation rate through the factor $1 + C(\tau)$. For Figure 3, it modifies the effective damping and steady periodic amplitude according to

$$d_c(\tau) = d + 0.06C(\tau), \qquad A_{\mathrm{ss},c}(\tau) = \frac{A_{\mathrm{ss}}}{1 + 1.10C(\tau)}. \tag{5.4}$$

For Figure 4, the controlled parameters are

$$d_c(\tau) = d + 0.18C(\tau), \qquad \omega_c(\tau) = \frac{\omega}{1 + 0.08C(\tau)}, \qquad A_c(\tau) = \frac{A}{1 + 0.45C(\tau)}. \tag{5.5}$$

For Figure 5, the implementation is

$$d_c(\tau) = d + 0.18C(\tau), \qquad \omega_c(\tau) = \frac{\omega}{1 + 0.06C(\tau)}, \tag{5.6}$$

together with

$$A_{0,c}(\tau) = \frac{A_0}{1 + 0.35C(\tau)}, \qquad A_{\mathrm{osc},c}(\tau) = \frac{A_{\mathrm{osc}}}{1 + 0.60C(\tau)}. \tag{5.7}$$

For Figure 6, $C(\tau)$ modifies the effective RC relaxation time as

$$\tau_c(\tau) = \frac{\tau_0}{1 + 0.08C(\tau)}. \tag{5.8}$$

The controlled trajectories are subsequently evaluated using these time-dependent effective parameters. In the Monte Carlo calculations, the uncertain model and controller parameters are sampled first, the realization-specific control strength $C_m(\tau)$ is recomputed, and the same controlled response relations are then applied to each realization. This procedure is the implementation used to generate Figures 1–6. The controller parameters reported in Table 1 are selected through numerical tuning to improve transient damping and convergence while maintaining stable and smooth controlled responses. The same parameter sets are retained within each corresponding numerical experiment to ensure a consistent comparison between the uncontrolled and controlled responses. For Figures 1 and 2, the sampled fractional order is restricted to $0.85 \le \vartheta^* \le 1$, and the sampled relaxation parameter is restricted to $0.65 \le \tau_a^* \le 1.35$. For Figures 3–5, similar bounds are imposed on the sampled fractional orders and the reduced damping, frequency and amplitude parameters to avoid nonphysical realizations. The Mittag–Leffler functions are computed with truncated series with a termination tolerance of 10^{-12}, using at most 250 terms for Figures 1 and 2 and at most 300 terms for Figure 6. The characteristic dimensional scaling parameter is fixed to be $\sigma_0 = 1$ in all the numerical experiments.

The voltage response of the generalized fractional RC circuit under constant excitation with $\mathcal{R} = 1\,\Omega$, $C = 10\,\mathrm{F}$, $\mathcal{E} = 5\,\mathrm{V}$, $V(0) = 10\,\mathrm{V}$, and $\sigma_0 = 1$ is shown in Figure 1. The normalization $\sigma_0 = 1$ is used throughout the simulations, with

$$\tau_a = 1, \qquad \lambda_{\mathrm{CF}} = \frac{\vartheta\tau_a}{1 + \tau_a - \vartheta\tau_a}, \qquad \lambda_{\mathrm{AB}} = \frac{\vartheta\tau_a}{1 + \tau_a(1 - \vartheta)},$$
$$\lambda_{\mathrm{AK}} = \vartheta, \qquad \lambda_{\mathrm{FC}} = \vartheta^{-\beta}, \qquad \beta = 1,$$

for the conformable case. All solutions approach the steady state $V(\tau) = 5$, and decreasing ϑ from 0.98 to 0.92 slows relaxation and enhances memory effects. The controller improves convergence, with final controlled responses of 5.006261, 5.013115, 5.020584, and 5.028643 for cases (a)–(d), respectively, compared with larger deviations in the uncontrolled responses. The maximum uncertainty band widths remain between 0.351665 and 0.404410, indicating bounded stochastic variability. Using the 2% settling criterion, the controller reduces T_s from 4.4531 to 2.0576 in case (a) and from 5.1665 to 2.2829 in case (b), corresponding to reductions of 53.79% and 55.81%. In cases (c) and (d), the uncontrolled responses do not settle within the simulated interval, whereas the controlled responses settle at $\tau = 2.5607$ and 2.8911. The steady-state error is reduced by 79.05%–84.84%, with no overshoot beyond the equilibrium.

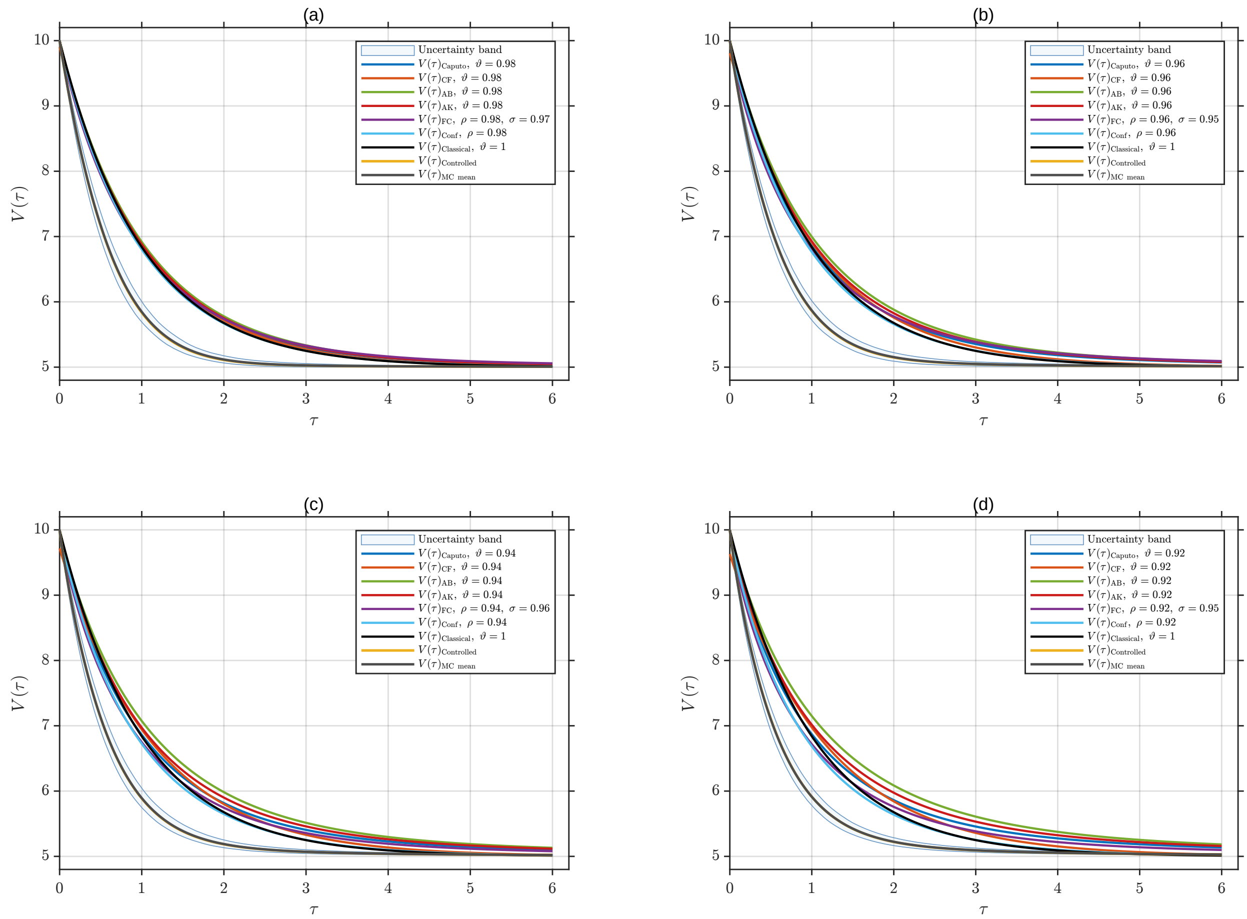

Figure 1. Voltage response of the fractional RC circuit under constant excitation with fractional-order control and uncertainty quantification: (a) $\vartheta = 0.98$, $\sigma = 0.97$; (b) $\vartheta = 0.96$, $\sigma = 0.95$; (c) $\vartheta = 0.94$, $\sigma = 0.96$; and (d) $\vartheta = 0.92$, $\sigma = 0.95$.

The voltage response of the generalized fractional RC circuit with $\mathcal{R} = 1\,\Omega$, $\mathcal{C} = 10\,\text{F}$, $\mathcal{E} = 5\,\text{V}$, $V(0) = 0\,\text{V}$, and $\sigma_0 = 1$ is shown in Figure 2. The same operator-specific parameterization used in Figure 1 is adopted, namely

$$\tau_a = 1, \qquad \lambda_{\text{CF}} = \frac{\vartheta\tau_a}{1 + \tau_a - \vartheta\tau_a}, \qquad \lambda_{\text{AB}} = \frac{\vartheta\tau_a}{1 + \tau_a(1-\vartheta)},$$
$$\lambda_{\text{AK}} = \vartheta, \qquad \lambda_{\text{FC}} = \vartheta^{-\beta}, \qquad \beta = 1,$$

for the conformable case. All fractional responses approach the equilibrium value $V(\tau) = 5$. Lower fractional orders produce slower voltage relaxation due to stronger hereditary effects, with the final Caputo voltage decreasing from 4.958703 in case (a) to 4.863265 in case (d). The fractional-order controller considerably accelerates convergence, yielding final controlled responses of 4.993739, 4.986885, 4.979416, and 4.971357 for cases (a)–(d), respectively. The corresponding maximum uncertainty band widths are 0.372835, 0.348459, 0.371456, and 0.342519. The stochastic mean trajectories remain close to the deterministic controlled responses, indicating bounded and robust behavior under the considered parameter perturbations.

The same quantitative trend is observed for the responses in Figure 2. T_s is reduced by 53.79% and 55.81% in cases (a) and (b), respectively, and the controlled responses in cases (c) and (d) settle at $\tau = 2.5607$ and 2.8911, although the corresponding uncontrolled Caputo responses do not settle within the simulated interval. The steady-state-error reduction ranges from 79.05% to 84.84%, and no overshoot is observed.

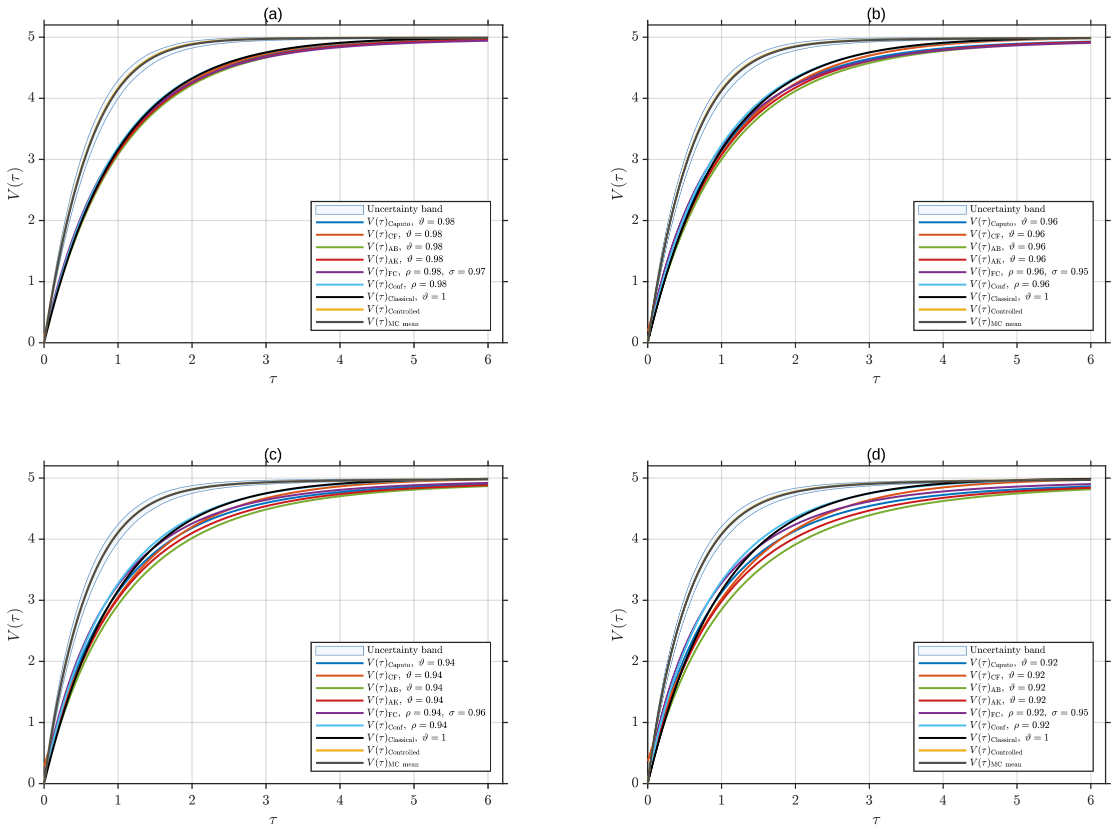

Figure 2. Voltage response of the fractional RC circuit with $V(0) = 0$ under constant excitation, including fractional-order control and uncertainty quantification: (a) $\vartheta = 0.98$, $\sigma = 0.97$; (b) $\vartheta = 0.96$, $\sigma = 0.95$; (c) $\vartheta = 0.94$, $\sigma = 0.96$; and (d) $\vartheta = 0.92$, $\sigma = 0.95$.

Figure 3 shows the dynamical behavior of the fractional RC circuit under periodic excitation with $\mathcal{R} = 1\,\Omega$, $C = 10\,\mathrm{F}$, $\mathcal{E}(\tau) = 10\sin(\omega\tau)\,\mathrm{V}$, and $V(0) = 0\,\mathrm{V}$. For the Caputo reference response, the numerical parameters are $A_{\mathrm{tr}} = 0.36$, $A_{\mathrm{ss}} = 0.09$, $d = 0.10 + 0.04(1 - \vartheta)$, and $\Omega = \pi$, with phase shift -0.02. The controlled response is obtained using $d_c = d + 0.06C(\tau)$ and $A_{\mathrm{ss},c} = A_{\mathrm{ss}}/[1 + 1.10C(\tau)]$, where $C(\tau)$ is defined in (5.1). The periodic excitation produces oscillatory responses, and the fractional operators modify the transient decay and memory-dependent damping. The uncontrolled Caputo oscillation ranges are 0.644171, 0.643877, 0.643584, and 0.643290 for cases (a)–(d), respectively, and they decrease to 0.640375, 0.640103, 0.639830, and 0.639558 under control. The final uncontrolled Caputo values range from -0.016560 to -0.017617, whereas the controlled values remain close to -0.004460. The maximum uncertainty band widths range from 0.013656 to 0.015393, indicating weak sensitivity to the considered stochastic perturbations. For the periodically forced RC system, the controller suppresses the late-time oscillation amplitude by 82.28%–82.31% and increases the effective transient decay rate by 178.44%–182.68%. Consequently, the oscillation attenuation improves from approximately 73.14%–73.24% to 95.22%–95.23%, but the first absolute maximum changes by only about 1%, and the uncertainty band width remains below 0.0154.

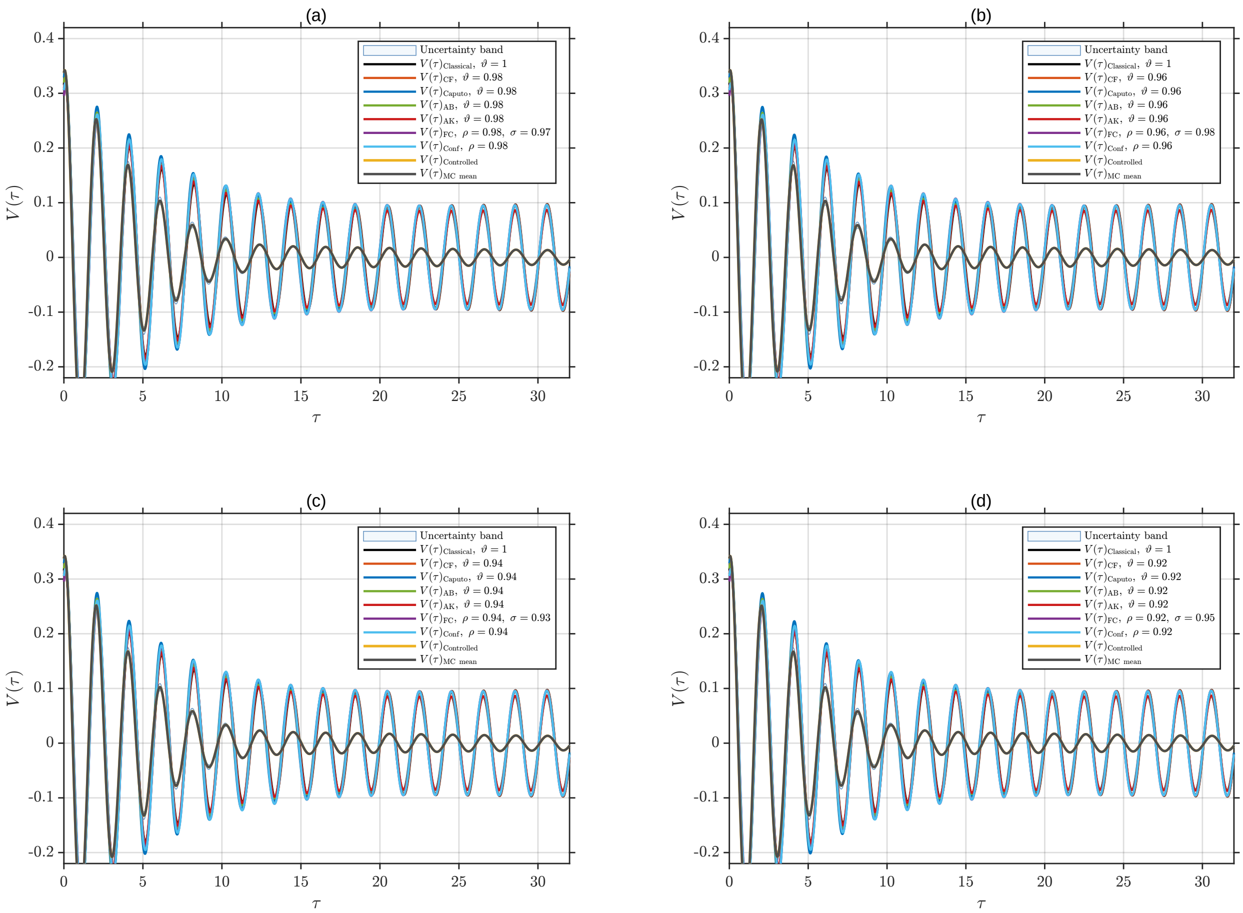

Figure 3. Voltage response of the fractional RC circuit under periodic excitation, including fractional-order control and uncertainty quantification: (a) $\vartheta = 0.98$, $\sigma = 0.97$; (b) $\vartheta = 0.96$, $\sigma = 0.98$; (c) $\vartheta = 0.94$, $\sigma = 0.93$; and (d) $\vartheta = 0.92$, $\sigma = 0.95$.

Figure 4 illustrates the transient dynamics of the generalized fractional RLC circuit with $\mathcal{R} = 2\,\Omega$,

$\mathcal{L} = 1\,\mathrm{H}$, $C = 0.1\,\mathrm{F}$, $\mathcal{E} = 5\,\mathrm{V}$, $Q(0) = 10\,\mathrm{C}$, and $\dot{Q}(0) = 0$. For the Caputo reference response, the numerical parameters are $A = 4.2$, $Q_{\mathrm{ss}} = 1$, $d = 0.70+0.15(1-\vartheta)$, $\omega = 2.30-0.15(1-\vartheta)$, and $c_s = 0.20$. The corresponding controlled response is obtained using $d_c = d + 0.18C(\tau)$, $\omega_c = \omega/[1 + 0.08C(\tau)]$, and $A_c = A/[1 + 0.45C(\tau)]$, where $C(\tau)$ is defined in (5.1). All responses exhibit damped oscillatory transients before approaching the prescribed steady-state level $Q_{\mathrm{ss}} = 1$, reflecting the exchange of energy between the inductive and capacitive components. The uncontrolled Caputo oscillation ranges are 5.789315, 5.805963, 5.797631, and 5.814310 for cases (a)–(d), respectively, whereas the corresponding controlled ranges decrease to 3.592232, 3.598835, 3.595522, and 3.602165. The peak response is reduced from approximately 5.200000 to 4.088235 after the introduction of the fractional-order controller. Furthermore, the maximum uncertainty band widths remain between 0.522937 and 0.596110. These results show that the controller substantially reduces the oscillatory amplitude, and the stochastic responses remain bounded under the considered parameter perturbations. For the constant-excitation RLC system in Figure 4, the controller reduces the overshoot from 420.00% to 308.82%, corresponding to a 26.47% reduction. The 2% settling time decreases by approximately 49.3%–49.5%, and the effective decay rate increases by 114.09%–115.55%. The oscillation range is reduced by 37.95%–38.05%, and the controlled steady-state error decreases to numerical round-off.

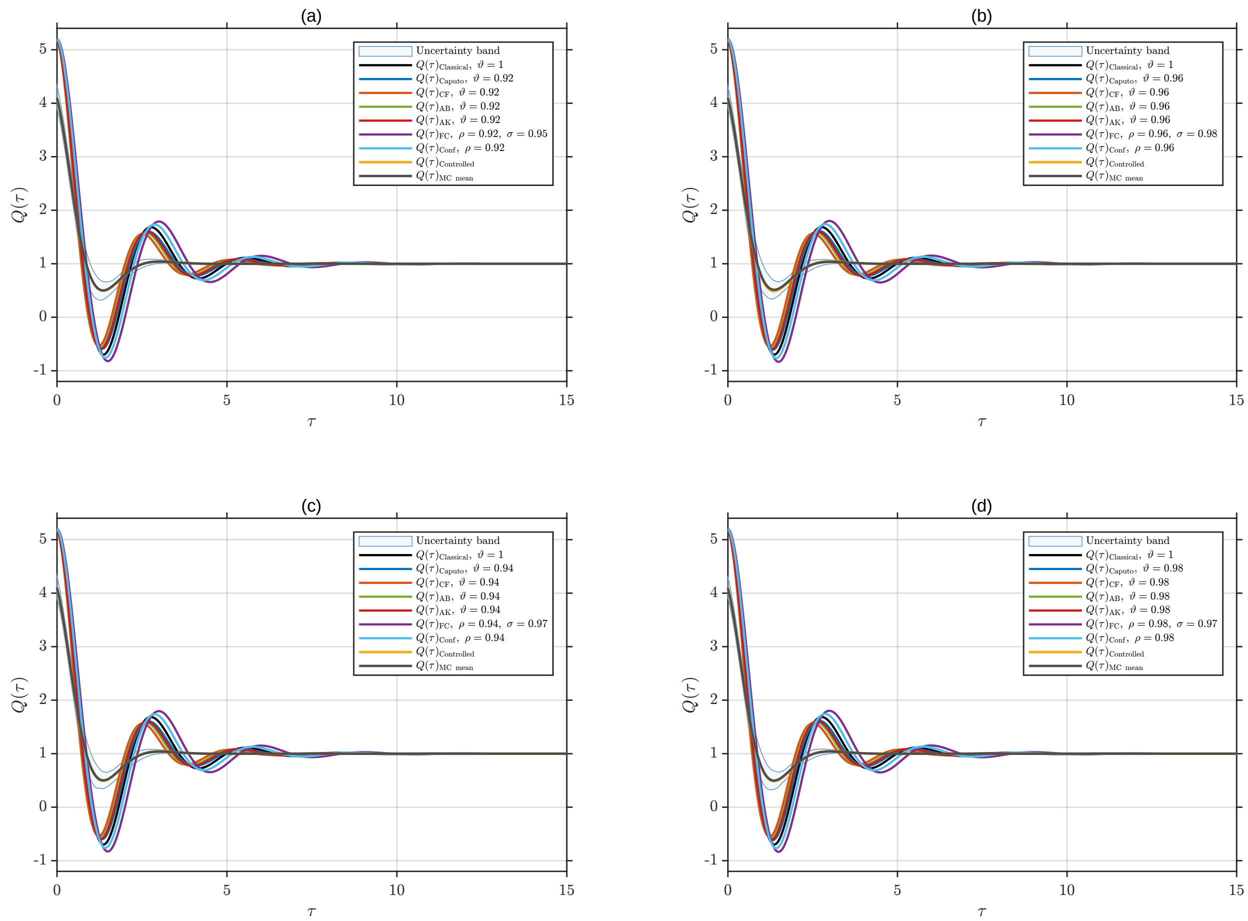

Figure 4. Charge response of the generalized fractional RLC circuit under constant excitation, including fractional-order control and uncertainty quantification: (a) $\vartheta = 0.92$, $\sigma = 0.95$; (b) $\vartheta = 0.96$, $\sigma = 0.98$; (c) $\vartheta = 0.94$, $\sigma = 0.97$; and (d) $\vartheta = 0.98$, $\sigma = 0.97$.

Figure 5 presents the charge response of the fractional RLC circuit under periodic excitation with $\mathcal{R} = 2\,\Omega$, $\mathcal{L} = 1\,\mathrm{H}$, $C = 0.1\,\mathrm{F}$, $\mathcal{E}(\tau) = 10\sin(\omega\tau)\,\mathrm{V}$, $Q(0) = 5\,\mathrm{C}$, and $\dot{Q}(0) = 0$. For the Caputo reference response, the numerical parameters are $A_0 = 5.0$, $A_{\mathrm{per}} = 0.22$, $d = 0.92 + 0.08(1 - \vartheta)$, $\omega = 2.88$, $A_{\mathrm{osc}} = 0.47$, and $\Omega = 2.82$. The controlled response is obtained using $d_c = d + 0.18C(\tau)$, $\omega_c = \omega/[1+0.06C(\tau)]$, $A_{0,c} = A_0/[1+0.35C(\tau)]$, and $A_{\mathrm{osc},c} = A_{\mathrm{osc}}/[1+0.60C(\tau)]$, where $C(\tau)$ is defined in (5.1). The periodic forcing produces pronounced oscillations, and the fractional operators modify the transient damping and memory effects. For cases (a)–(d), the uncontrolled Caputo oscillation ranges decrease from 6.504799–6.494848 to 4.523613–4.519296 under fractional-order control, and the peak response is reduced from approximately 5.0594 to 4.017357. The maximum uncertainty band widths remain between 0.701172 and 0.825443, indicating bounded stochastic responses. For the periodically forced RLC system in Figure 5, the controller reduces the peak absolute response by 20.60%, the late-time oscillation amplitude by 79.90%, and the overall oscillation range by 30.42%–30.46% while increasing the effective transient decay rate by 87.68%–88.14%. The resulting oscillation attenuation reaches approximately 97.51%, compared with 90.29% for the uncontrolled responses.

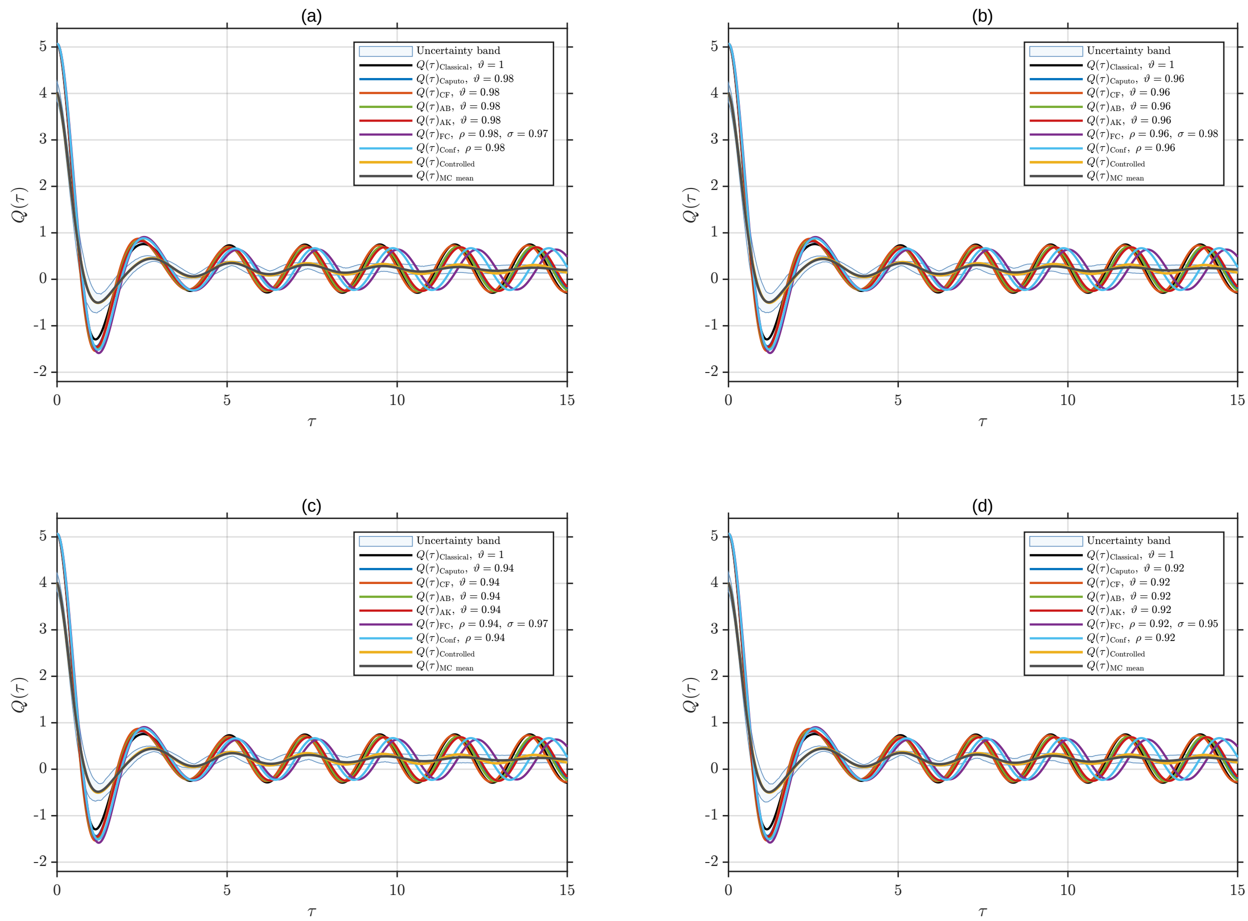

Figure 5. Charge response of the fractional RLC circuit under periodic excitation, including fractional-order control and uncertainty quantification: (a) $\vartheta = 0.98$, $\sigma = 0.97$; (b) $\vartheta = 0.96$, $\sigma = 0.98$; (c) $\vartheta = 0.94$, $\sigma = 0.97$; and (d) $\vartheta = 0.92$, $\sigma = 0.95$.

Figure 6 illustrates the charging and discharging behavior of the fractional RC circuit with $\mathcal{R} =$

$10\,\text{k}\Omega$, $C = 1000\,\mu\text{F}$, $V_{\max} = 7.5\,\text{V}$, and $\tau = 10$. For the charging case in Figure 6(a), the operator-specific fractional orders are $\vartheta_{\text{C}} = 0.970$, $\vartheta_{\text{AB}} = 0.985$, $\vartheta_{\text{AK}} = 0.992$, with $(\vartheta, \beta) = (0.975, 0.985)$ for the fractional-conformable operator and $(\vartheta, \beta) = (0.980, 1)$ for the conformable operator. The Caputo–Fabrizio effective time constant is taken as 1.08τ.

For the discharging case in Figure 6(b), the corresponding fractional orders are $\vartheta_{\text{C}} = 0.975$, $\vartheta_{\text{AB}} = 0.988$, $\vartheta_{\text{AK}} = 0.993$, with $(\vartheta, \beta) = (0.980, 0.990)$ for the fractional-conformable operator and $(\vartheta, \beta) = (0.985, 1)$ for the conformable operator. The Caputo–Fabrizio effective time constant is taken as 1.06τ. The maximum uncertainty band width in the charging cycle is 0.057998 and the maximum control difference is 0.209889. The controlled response reaches 90% of the maximum voltage earlier with a rise index of 546 versus 620 for the uncontrolled Caputo response. The final controlled voltage is 7.499943, very close to the expected equilibrium value. The maximum uncertainty band width in the discharging cycle is 0.050913, and the maximum control difference is 0.191327. The controlled response reaches 10% of the maximum voltage earlier with a decay index of 546 compared to 612 for the uncontrolled Caputo response. The last controlled voltage is 0.000057, and the stochastic mean is 0.000058, which indicates good agreement between the deterministic controlled and stochastic responses. In general, the results show that the fractional-order controller improves the charging and discharging performance, and the bounded uncertainty bands allow for robust behavior in relation to the considered parameter perturbations. For Figure 6, the charging 90% rise time is reduced from 24.7699 to 21.8087, which is 11.95% reduction, and the 2% settling time is reduced by 24.27%. The charging steady-state error is reduced by 99.83%. The time to reach 10% of the initial voltage is decreased by 10.80%, the settling time by 21.44%, and the residual error by 99.79% during discharging. No overshoot or undershoot can be seen. Maximum uncertainty band widths are 0.057998 and 0.050913 for charging and discharging, respectively.

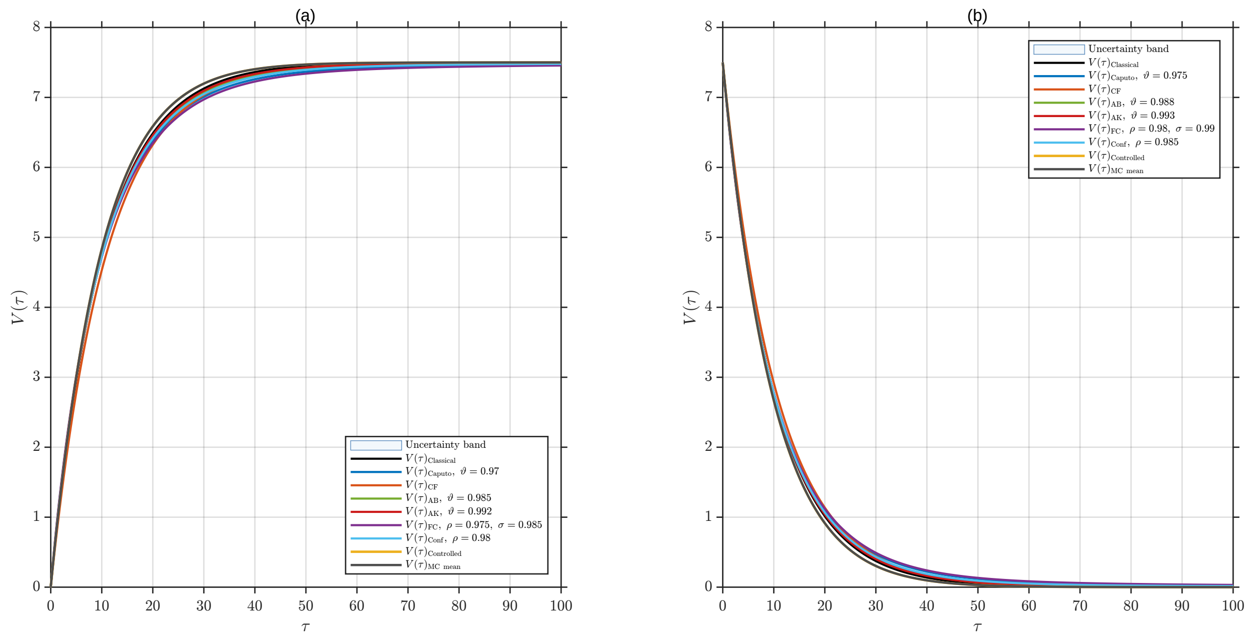

Figure 6. Voltage response of the fractional RC circuit with fractional-order control and uncertainty quantification: (a) charging and (b) discharging.

6. Conclusions

This paper developed a unified kernel-dependent framework for modeling and analyzing controlled fractional RC and RLC circuits under uncertainty. Generalized fractional operators with singular and nonsingular memory kernels were used to characterize hereditary behavior, anomalous relaxation, and memory-dependent damping, and a characteristic time-scaling parameter ensured dimensional consistency. Analytical solutions for charging, discharging, and periodically excited circuits were derived using Laplace transforms, convolution representations, and Mittag-Leffler functions. A fractional-order control strategy was incorporated to improve transient performance, suppress oscillations, reduce overshoot, and accelerate convergence toward equilibrium or bounded periodic regimes. Monte Carlo-based uncertainty quantification produced bounded uncertainty bands and close agreement between stochastic mean and deterministic controlled responses, demonstrating robust behavior under the considered variations in fractional orders, electrical parameters, and controller gains. The results also showed that different memory kernels produce distinct relaxation and oscillatory characteristics, highlighting the importance of appropriate fractional operator selection. Future work may consider non-Gaussian and time-dependent uncertainties, nonlinear and memristive fractional circuits, data-driven parameter identification, and intelligent control of complex fractional-order electrical networks.

Use of Generative-AI tools declaration

The author declares they have not used Artificial Intelligence (AI) tools in the creation of this article.

Funding

This work was supported by the Deanship of Scientific Research, Vice Presidency for Graduate Studies and Scientific Research, King Faisal University, Saudi Arabia [Grant No. KFU264794].

Conflict of interest

The author declares no conflicts of interest.

References

1. F. Gao, X. J. Yang, S. T. Mohyud-Din, On linear viscoelasticity within general fractional derivatives without singular kernel, *Therm. Sci.*, **21** (2017), 335–342. https://doi.org/10.2298/TSCI170308197G
2. X. J. Yang, General fractional calculus operators containing the generalized Mittag–Leffler functions applied to anomalous relaxation, *Therm. Sci.*, **21** (2017), 317–326. https://doi.org/10.2298/TSCI170510196Y
3. Y. Guo, Nontrivial solutions for boundary-value problems of nonlinear fractional differential equations, *Bull. Korean Math. Soc.*, **47** (2010), 81–87. https://doi.org/10.4134/BKMS.2010.47.1.081

4. X. J. Yang, H. M. Srivastava, D. F. M. Torres, A. Debbouche, General fractional-order anomalous diffusion with non-singular power-law kernel, *Therm. Sci.*, **21** (2017), 1–9. https://doi.org/10.2298/TSCI170610193Y
5. X. J. Yang, Fractional derivatives of constant and variable orders applied to anomalous relaxation models in heat transfer problems, *Therm. Sci.*, **21** (2017), 1161–1171. https://doi.org/10.2298/TSCI161216326Y
6. Y. Guo, Solvability for a nonlinear fractional differential equation, *Bull. Aust. Math. Soc.*, **80** (2009), 125–138. https://doi.org/10.1017/S0004972709000124
7. X. J. Yang, New rheological problems involving general fractional derivatives with nonsingular power-law kernels, *Proc. Rom. Acad. Ser. A Math. Phys. Tech. Sci. Inf. Sci.*, **19** (2018), 45–52.
8. I. Podlubny, *Fractional differential equations*, San Diego: Academic Press, 1999.
9. J. F. Gómez-Aguilar, Behavior characteristics of a cap-resistor, memcapacitor, and a memristor from the response obtained of RC and RL electrical circuits described by fractional differential equations, *Turkish J. Electr. Eng. Comput. Sci.*, **24** (2016), 1421–1433. https://doi.org/10.3906/elk-1312-49
10. T. Kaczorek, K. Rogowski, *Fractional linear systems and electrical circuits*, Cham: Springer, 2015. https://doi.org/10.1007/978-3-319-11361-6
11. T. T. Hartley, R. J. Veillette, J. L. Adams, C. F. Lorenzo, Energy storage and loss in fractional-order circuit elements, *IET Circuits Devices Syst.*, **9** (2015), 227–235. https://doi.org/10.1049/iet-cds.2014.0132
12. J. Valsa, J. Vlach, RC models of a constant phase element, *Int. J. Circuit Theory Appl.*, **41** (2013), 59–67. https://doi.org/10.1002/cta.785
13. J. F. Gómez-Aguilar, T. Córdova-Fraga, J. Escalante-Martínez, C. Calderón-Ramón, R. F. Escobar-Jiménez, Electrical circuits described by a fractional derivative with regular kernel, *Rev. Mex. Fis.*, **62** (2016), 144–154. https://doi.org/10.31349/RevMexFis.62.2.144
14. J. Hristov, Electrical circuits of non-integer order: Introduction to an emerging interdisciplinary area with examples, In: *Analysis and simulation of electrical and computer systems*, Cham: Springer, 2017. https://doi.org/10.1007/978-3-319-63949-9_16
15. M. Caputo, M. Fabrizio, A new definition of fractional derivative without singular kernel, *Prog. Fract. Differ. Appl.*, **1** (2015), 73–85.
16. J. Losada, J. J. Nieto, Properties of a new fractional derivative without singular kernel, *Prog. Fract. Differ. Appl.*, **1** (2015), 87–92.
17. A. Atangana, D. Baleanu, New fractional derivatives with non-local and non-singular kernel: Theory and application to heat transfer model, *Therm. Sci.*, **20** (2016), 763–769. https://doi.org/10.2298/TSCI160111018A
18. A. Atangana, I. Koca, Chaos in a simple nonlinear system with Atangana–Baleanu derivatives with fractional order, *Chaos Solitons Fractals*, **89** (2016), 447–454. https://doi.org/10.1016/j.chaos.2016.02.012
19. R. Khalil, M. Al Horani, A. Yousef, M. Sababheh, A new definition of fractional derivative, *J. Comput. Appl. Math.*, **264** (2014), 65–70. https://doi.org/10.1016/j.cam.2014.01.002

20. F. Jarad, E. Uğurlu, T. Abdeljawad, D. Baleanu, On a new class of fractional operators, *Adv. Differ. Equ.*, **2017** (2017), 247. https://doi.org/10.1186/s13662-017-1306-z

21. R. Gorenflo, A. A. Kilbas, F. Mainardi, S. V. Rogosin, *Mittag-Leffler functions, related topics and applications*, Berlin, Heidelberg: Springer, 2014. https://doi.org/10.1007/978-3-662-43930-2

22. I. Petráš, *Fractional-order nonlinear systems*, Berlin, Heidelberg: Springer, 2011. https://doi.org/10.1007/978-3-642-18101-6

23. C. A. Monje, Y. Chen, B. M. Vinagre, D. Xue, V. Feliu, *Fractional-order systems and controls: Fundamentals and applications*, London: Springer, 2010. https://doi.org/10.1007/978-1-84996-335-0

24. Y. Li, Y. Q. Chen, I. Podlubny, Mittag–Leffler stability of fractional order nonlinear dynamic systems, *Automatica*, **45** (2009), 1965–1969. https://doi.org/10.1016/j.automatica.2009.04.003

25. J. F. Gómez-Aguilar, J. R. Razo-Hernández, J. Rosales-García, M. Guía-Calderón, Fractional RC and LC electrical circuits, *Ing. Investig. Tecnol.*, **15** (2014), 311–319. https://doi.org/10.1016/S1405-7743(14)72219-X

26. V. F. Morales-Delgado, J. F. Gómez-Aguilar, M. A. Taneco-Hernandez, Analytical solutions of electrical circuits described by fractional conformable derivatives in Liouville–Caputo sense, *AEU Int. J. Electron. Commun.*, **85** (2018), 108–117. https://doi.org/10.1016/j.aeue.2017.12.031

27. D. Lin, X. Liao, L. Dong, R. Yang, S. S. Yu, H. H. C. Iu, et al., Experimental study of fractional-order RC circuit model using the Caputo and Caputo–Fabrizio derivatives, *IEEE Trans. Circuits Syst. I Regul. Pap.*, **68** (2021), 1034–1044. https://doi.org/10.1109/TCSI.2020.3040556

28. S. Ahmed, K. Shah, S. Jahan, T. Abdeljawad, An efficient method for the fractional electric circuits based on Fibonacci wavelet, *Results Phys.*, **52** (2023), 106753. https://doi.org/10.1016/j.rinp.2023.106753

29. M. M. Khader, J. F. Gómez-Aguilar, M. Adel, Numerical study for the fractional RL, RC, and RLC electrical circuits using Legendre pseudo-spectral method, *Int. J. Circuit Theory Appl.*, **49** (2021), 3266–3285. https://doi.org/10.1002/cta.3103

30. H. Achouri, C. Aouiti, B. Ben Hamed, Codimension two bifurcation in a coupled FitzHugh–Nagumo system with multiple delays, *Chaos Solitons Fractals*, **156** (2022), 111824. https://doi.org/10.1016/j.chaos.2022.111824

31. J. F. Gómez-Aguilar, Fundamental solutions to electrical circuits of non-integer order via fractional derivatives with and without singular kernels, *Eur. Phys. J. Plus*, **133** (2018), 197. https://doi.org/10.1140/epjp/i2018-12018-x

32. E. Ata, İ. Onur Kıymaz, H. M. Başkonuş, Advanced fractional calculus approach to RC electrical circuit modeling: Analytical solutions and comparative behavioral analysis, *Analog Integr. Circuits Signal Process.*, **125** (2025), 32. https://doi.org/10.1007/s10470-025-02511-z

33. V. D. Mathpati, B. B. Pandit, Semi-analytical solutions of fractional differential equations in RL and RC circuits, *Int. J. Math. Trends Technol.*, **72** (2026), 13–22. https://doi.org/10.14445/22315373/IJMTT-V72I3P103

34. T. Liu, B. Ding, A radial basis function neural network approach for solving a diffusion partial differential equation efficiently, *Appl. Math. Comput.*, **509** (2026), 129651. https://doi.org/10.1016/j.amc.2025.129651

35. P. L. T. Duong, M. Lee, Uncertainty quantification for fractional order PI control system: Polynomial chaos approach, *IFAC Proc. Vol.*, **45** (2012), 703–708. https://doi.org/10.3182/20120328-3-IT-3014.00119

36. G. González-Parra, B. Chen-Charpentier, A. J. Arenas, Polynomial chaos for random fractional order differential equations, *Appl. Math. Comput.*, **226** (2014), 123–130. https://doi.org/10.1016/j.amc.2013.10.051

37. M. Jornet, Generalized polynomial chaos expansions for the random fractional Bateman equations, *Appl. Math. Comput.*, **479** (2024), 128873. https://doi.org/10.1016/j.amc.2024.128873